

Engineered Cementitious Composites (ECC) – Material, Structural, and Durability Performance

Victor C. Li
University of Michigan, Ann Arbor, MI 48109

August 30, 2007

~~Book Chapter in *Concrete Construction Engineering Handbook*, Ed. E. Nawy, to be published by CRC Press, 2007.~~ [λ](#)

Engineered Cementitious Composites (ECC) – Material, Structural and Durability Performance

by

Victor C. Li, Ph.D., FASCE, FASME, FWIF

E. Benjamin Wylie Collegiate Chair Professor of the department of Civil and Environmental Engineering, University of Michigan, Ann Arbor. An expert on high performance fiber reinforced cementitious composites, he is the inventor of ECC.

24.1	Historical Development	2
24.2	General Characteristics.....	4
24.2.1	The Family of ECC Materials	4
24.2.2	Tensile Characteristics	5
24.2.3	ECC Material Design Considerations.....	6
24.2.4	Compressive and Flexural Characteristics.....	8
24.3	Mixture Proportioning, Material Processing and Quality Control	8
24.4	Behavior of ECC Structural Elements.....	11
24.4.1	Structural Response of R/ECC Elements.....	12
24.4.1.1	Flexural Elements	12
24.4.1.2	Shear Element.....	13
24.4.1.3	Column Element	13
24.4.1.4	Beam-Column Connection Element	13
24.4.1.5	Wall Panel Element.....	14
24.4.2	Insights from R/ECC element response.....	14
24.4.2.1	Potential for reduction or elimination of shear reinforcement	14
24.4.2.2	Damage tolerance.....	14
24.4.2.3	Compatible deformation between ECC and reinforcement.....	15
24.4.2.4	Tight crack width control and elimination of crack control reinforcement 15	
24.4.2.5	Transforming material ductility into structural strength	16
24.5	Durability of ECC and ECC Structural Elements	16
24.5.1	Material and Element Durability	16
24.5.2	ECC Durability Under Various Environments.....	18
24.5.2.1	Long Term Tensile Strain Capacity	18
24.5.2.2	Freeze Thaw Durability.....	18
24.5.2.3	Tropical Climate Exposure.....	19
24.5.2.4	Chloride Immersion	19
24.5.2.5	Deicing Salt Exposure.....	19
24.5.2.6	Alkali-silicate Reaction Resistance.....	20
24.5.3	Durability of R/ECC	20
24.5.3.1	Transport Properties of ECC	21
24.5.3.2	Corrosion Resistance in R/ECC.....	23
24.5.4	Long Term Performance	25
24.6	Concluding Remarks	26

24.1 Historical Development

The development of fiber reinforced concrete material has undergone a number of phases. In the 1960's, research by Romauldi and co-workers (e.g. Romauldi and Batson, 1963; Romauldi and Mandel, 1964) demonstrated the effectiveness of short steel fibers in reducing the brittleness of concrete. This development has continued with expansion to a variety of other fibers, such as glass, carbon, synthetics, natural fibers and in recent years, hybrids that combine either different fiber types or fiber lengths. The continuously enhanced knowledge of fiber reinforcement effectiveness has resulted in structural design recommendations by RILEM TC 162-TDF (Vandewalle et al, 2003). This document focuses on fiber reinforced concrete (FRC) that possesses a tension-softening quasi-brittle response (Figure 24.1). Apart from the gradual expanded use of the tension-softening branch of FRC in structural property enhancements, fibers in small dosage have been successfully used in controlling restrained drying shrinkage cracks. The subject of FRC is treated in detail in Chapter 22A of this book.

Beginning as early as the 1980's, interest in creating a fiber reinforced concrete material with tensile ductility has been gaining ground. Within FRC, the toughness of the material is increased, but no change in ductility is attained. Ductility is a measure of tensile deformation (strain) capacity typically associated with ductile steel, for example, but not with concrete material. Attempts in achieving tensile ductility in concrete material are exemplified by the early efforts of Aveston et al. (1971), and later Krenchel and Stang (1989) who demonstrated that with continuous aligned fibers, high tensile ductility hundreds of times that of normal concrete can be attained. The modern day version of continuous fiber reinforcement is represented by textile reinforced concrete materials that may be prestressed (Reinhardt et al, 2003; Curbach and Jesse, 1999). Research on pultruded continuous fiber reinforced concrete was pioneered by Mobasher et al (2006). Developed in parallel, the use of discontinuous fibers at high dosage (4-20%) such as in cement laminates (Allen, 1971) and in SIFCON (Slurry Infiltrated Fiber CONcrete) (Lankard, 1986; Naaman, 1992) has resulted in concrete composite materials that attain higher tensile strength than normal concrete and which are not as brittle, but with much less ductility than their continuous fiber and textile reinforced counterparts.

These materials may be considered a class of materials separate from FRC in that different degrees of tensile ductility are achieved, often accompanied by a strain hardening response distinct from the tension-softening response of FRC. Naaman and Reinhardt (2003) classified such material as High Performance Fiber Reinforced Cementitious Composites (HPFRCC) (Figure 24.1). It should be noted that most members of this class of material have a matrix that does not contain coarse aggregates, and should therefore be regarded as fiber reinforced cement pastes or mortars. However, in keeping with the broadened meaning used in the literature, we shall use the term "concrete material" in this chapter to include concrete, mortar, and cement paste.

Figure 24.1 illustrates schematically the differences between the tensile response of normal concrete, FRC, and HPFRCC, such as obtained from a uniaxial tension test. This figure emphasizes the transition from brittle concrete to quasi-brittle FRC (tension-softening) to ductile HPFRCC (strain-hardening). Specifically, during tension-softening, deformation is localized onto a single fracture plane, most appropriately described in terms of crack opening. During strain-hardening, deformation is composed of the opening of multiple subparallel fine cracks, and elastic stretching of the material between these cracks. Over a length scale that includes many such cracks, the deformation may be considered tensile “strain” smeared over a representative volume of material. As will be seen in the following sections, these distinctions between FRC and HPFRCC have significant ramifications in terms of load capacity and structural durability.

While the HPFRCC materials mentioned above embody the highly desired tensile properties lacking in normal concrete or in FRC, until recently they have mostly been limited to academic research laboratories or specialized applications. This is due to additional demands in industrial projects, particularly in on-site construction, such as economical feasibility and constructability. These two demands are difficult to meet when either continuous fibers or high fiber content are used in the composites.

In recent years, two new classes of HPFRCC have emerged. Ductal[®] has high tensile strength of 12MPa and a ductility of 0.02-0.06% (Chanvillard and Rigaud, 2003), and ECC originally developed at the University of Michigan, with a typical moderate tensile strength of 4-6MPa and a higher ductility of 3-5% (Li, 1993; Fischer et al, 2003). The tensile stress-strain curves of these two types of HPFRCCs are illustrated in Figure 24.2. The development approach for these two classes of materials is quite different. For Ductal, which can be traced back to the work of Bache (1981), the approach is to employ a tightly packed dense matrix to increase both tensile and compressive strength of the material. Fiber is added to counteract the resulting high brittleness of the densified matrix. The dense matrix allows a strong bond with the fiber that results in a high post-cracking strength as long as a fiber with high strength is utilized. For ECC, the approach is to create synergistic interactions between fiber, matrix and interface, to maximize the tensile ductility by development of closely spaced multiple microcracks while minimizing the fiber content (generally 2% or less by volume). This approach is detailed in Section 24.2.3. Ductal is designed for use in the elastic stage, so that the fiber action becomes effective only when the structural ultimate limit state (ULS) is approached. ECC is generally designed for use in the elastic and strain-hardening (inelastic) stages, so that fiber action becomes effective even under normal service loads.

The development of ECC is still evolving, even though a number of full-scale structural applications have already appeared in Japan, Europe and the US. This article summarizes some basic knowledge of ECC. In the following, the fundamental characteristics of ECC are described. This is followed by a section on structural behavior of steel reinforced ECC elements (R/ECC), and a section on durability behavior of ECC material and R/ECC.

The literature on ECC is rapidly expanding with contributions from academic research and industrial organizations around the world. Some good sources of references include recent workshop or conference proceedings on this subject, e.g. HPFRCC in Structural Applications (Fischer and Li, 2006), FRAMCOS-6 (Carpinteri et al, 2007) and HPFRCC 5 (Reinhardt and Naaman, 2007). These documents contain a number of papers on ECC and related subjects. In assisting the transition to broader industrial use, the Japan Society of Civil Engineers has published a design guideline (JSCE 2007; Rokugo et al, 2007), and the RILEM TC HFC technical committee will be publishing two state of the art reports on this subject. To aid the reader in maneuvering this literature, some clarification on semantics will be helpful. The name Engineered Cementitious Composites (ECC) was adopted by the original developers (Li, 1993) to emphasize the micromechanics basis behind the design of this material. Micromechanics serves as a powerful tool to guide materials design for targeted composite properties, and enables a meaningful linkage between materials engineering and structure performance design (Li, 2007). In 2006, the RILEM TC HFC technical committee decided to emphasize the unique tensile strain-hardening response of this material (Figure 24.1) as a constitutive law for structural engineering design, and gave the more descriptive name Strain Hardening Cementitious Composites (SHCC) to this class of materials. JSCE, however, prefers to emphasize the multiple fine cracking (and associated durability, see Section 24.5), thus naming the material as “Multiple Fine Cracking Fiber Reinforced Cementitious Composites”. In essence, all of these materials are designed using micromechanical tools and represent identical material technology.

24.2 General Characteristics

24.2.1 *The Family of ECC Materials*

ECC can be regarded as a family of materials with a range of tensile strengths and ductilities that can be adjusted depending on the demands of a particular structure. ECC also represents a family of materials with different functionalities in addition to the common characteristics of high tensile ductility and fine multiple cracking. Self-consolidating ECC (e.g. ECC M45 and its variants) is designed for large-scale on-site construction applications (Kong et al, 2003; Lepech and Li, 2007). High early strength ECC (HES-ECC) is designed (Wang and Li, 2006a) for applications which require rapid strength gain such as transportation infrastructure that needs fast reopening to the motorist public. Light-weight ECC (LW-ECC) is designed (Wang and Li, 2003) for applications where the dead load of structural members must be minimized. Green ECC (G-ECC) is designed (Li et al, 2004, Lepech et al, 2007) to maximize material greenness and infrastructure sustainability. Self-healing ECC (SH-ECC) emphasizes the functionality of recovering transport and mechanical properties after experiencing damage (Yang et al, 2005; Li and Yang, 2007).

ECC using local material ingredients have been successfully produced in various countries, including Japan (Kanda et al, 2006), Europe (Mechtcherine and Schulze, 2006), and S. Africa (Boshoff and van Zijl, 2007), in addition to the US. To successfully

develop local versions of ECC, a good understanding of the underlying design approach (Li, 1993; Kanda and Li, 1999) is helpful. A synopsis of the ECC design approach is given in Section 24.2.3.

A summary of major physical properties of ECC is given in Table 24.1 below. It should be emphasized that ECC properties are tailorable through the use of micromechanics tools. Even broader ranges of properties beyond those in this table can be expected in future as the need arises.

Table 24.1: Major physical properties of ECC

Compressive Strength (MPa)	First Crack Strength (MPa)	Ultimate Tensile Strength (MPa)	Ultimate Tensile Strain (%)	Young's Modulus (GPa)	Flexural Strength (MPa)	Density (g/cc)
20 – 95	3 – 7	4 – 12	1 – 8	18 – 34	10 – 30	0.95 – 2.3

The very high strength and modulus version was attained by Kamal et al (2007). The very high tensile ductility version was reported in Li et al (1996). The super light-weight version was described in Wang and Li (2003). The common characteristic of these ECC materials is that they have tensile ductility orders of magnitude higher than those in typical concrete or FRC materials.

It should be noted that while a large body of literature has developed around ECC based on PVA fiber, commonly referred to as PVA-ECC, other fibers have been successfully utilized. These include high modulus polyethylene (PE) fibers (Li, 1993; Li and Wang, 2002; Kamal et al, 2007) and polypropylene (pp) fibers (Takashima et al, 2003; Yang and Li, 2007). The principle behind the design of ECC as discussed in Section 24.2.3 does not depend on a particular fiber. Fibers with certain properties, however, may meet the criteria for tensile strain-hardening at a lower volume fraction. Decisions on what fibers to use will depend on their natural characteristics, including mechanical, diameter ranges, and surface characteristics, on resulting ECC mechanical, durability, and sustainability performances and on economics.

24.2.2 Tensile Characteristics

As indicated earlier, the most important characteristic of ECC is the high tensile ductility represented by a uniaxial tensile stress-strain curve with strain capacity as high as 5% (Figures 24.2(b,c) and 24.3). This metal like behavior shows a characteristic “yield point” at the end of the elastic stage when the first microcrack appears on the specimen. Subsequent increase in load results in a strain-hardening response, i.e. a rise in tensile deformation (volumetric straining in the form of multiple microcracking as opposed to localized crack opening) accompanied by a rise in load. Final failure of the specimen occurs when one of the multiple cracks forms a fracture plane. Beyond this peak load, ECC is no different than normal FRC, showing a tension-softening response. The high tensile ductility is of great value in enhancing the structural ultimate limit state (ULS) in terms of structural load and deformation capacity as well as energy absorption. In this

manner, ECC can offer structural safety improvements. This contribution of ECC to structural response enhancement is discussed further in Section 24.4.

The formation of multiple microcracking is necessary to achieve high composite tensile ductility. Between first cracking strain (about 0.01%) and 1% strain, the microcrack opening increases from zero to about 60 μm . Further loading beyond 1% causes more multiple cracks to form, but with no additional crack opening beyond the steady state value of 60 μm (Figure 24.3). Governed by the mechanics of the fiber-matrix interaction within ECC, this unique characteristic is critically important for durability (see Section 24.5) of both material and structure. Unlike concrete or FRC, the steady state crack width is an intrinsic material property, independent of loading (tension, bending or shear), structure size and geometry, and steel reinforcement type and amount. This observation has important implications in service life, maximum member size, economics, and architectural aesthetics. In short, where steel reinforcement is used to control crack width in concrete, such steel reinforcement can be completely eliminated in ECC. By suppressing cracks with large crack width even in the presence of large imposed structural deformations, ECC can offer structural durability improvements in addition to water tightness and other serviceability enhancements.

Although Figure 24.3 shows a particular example of ECC with steady state crack width at 60 μm , even tighter crack widths, as low as 20 μm , have been achieved (Yang et al, 2007).

24.2.3 ECC Material Design Considerations

In order to attain high tensile ductility and tight microcrack width, while keeping the fiber content low (2% or less by volume), ECC has been optimized through the use of micromechanics (Li and Leung, 1992; Li, 1993). Micromechanics is a branch of mechanics applied at the material constituent level, and captures the mechanical interactions between the fiber, mortar matrix and fiber/matrix interface. Typically, fibers are of the order of millimeters in length, tens of microns in diameter, and may have a surface coating on the nanometer scale. Matrix heterogeneities in ECC, including defects, sand particles, cement grains, and mineral admixture particles, have size ranges from nano-scale to mm-scale. Ideally, the micromechanics model should capture all the deformation mechanisms at the mm, μm , and nanometer scales. However, simplifying assumptions have been made to make the model equations tractable, and that the resulting conditions (in closed-form solution) for strain-hardening can be used as guidelines for material component tailoring. These conditions are expressed in strength and energy terms, as shown in Eq. (24.1).

Strength criterion

$$\sigma_0 \geq \sigma_{cs} \quad (24.1a)$$

Energy criterion

$$J'_b \equiv \sigma_0 \delta_0 - \int_0^{\delta_0} \sigma(\delta) d\delta \geq J_{tip} \approx \frac{K_m^2}{E_m} \quad (24.1b)$$

where σ_{cs} and σ_0 are the cracking strength and maximum fiber bridging capacity on each potential crack plane, δ_0 is the crack opening corresponding to σ_0 in the fiber bridging relationship $\sigma(\delta)$ which goes through a maximum, and J_{tip} and J'_b are the crack tip matrix toughness and the complimentary energy of the fiber bridging relation, respectively. K_m and E_m are the matrix fracture toughness and Young's Modulus, respectively. For derivation of Eq. 24.1, see Li (1993). Physically, the strength criterion Eq. (24.1a) ensures the initiation of microcracks from initial flaw sites in the composite before the tensile load exceeds the maximum fiber bridging capacity. The left hand side of Eq. (24.1a) can be thought of as the maximum tensile load carried by a line of springs with tensile strength determined by the bridging fibers. Failure of the fiber springs is associated with fiber rupture, slippage, and/or pull-out. Ensuring that the maximum fiber bridging capacities on existing crack planes remain higher than the matrix cracking strength of potential new crack planes allows additional cracks to form. Otherwise, saturated multiple cracking would not be attained, and sparsely spaced cracks will result, limiting the tensile ductility.

The energy criterion Eq. (24.1b) prescribes the mode of crack propagation once initiated. The normal form of Griffith cracking is not favorable to multiple cracking. This is because the crack opening in Griffith-type cracks, especially at the mid point of the crack line δ_m , always increases with the length of the crack, and failure of the bridging fiber invariably results either in the form of fiber pull-out or breakage beginning at this widest point when δ_m exceeds δ_0 . The only means of preventing this is by altering the Griffith crack propagation mode to a flat crack propagation mode whereby the crack extends while the crack opening stay constant at any location (apart from a small bridging zone near the crack tip) regardless of the length of the crack. In this manner, δ_m stays below δ_0 along the whole crack line. During flat crack propagation, energy is exchanged between work input (from applied loading) and energy absorbed by the fiber bridging process in the opening of the crack near the crack tip (and only near the crack tip), as well as matrix material breakdown at the crack tip. The enforcement of energy balance results in Eq. 24.1b. Violation of Eq. (24.1b) results in fracture localization as in the case of FRC, and terminates the multiple cracking process. The energy criterion is schematically illustrated in Figure 24.4.

It should be noted that both parts of Eq. (24.1) have been arranged so that the left hand sides of the inequality sign contain terms that pertain to fiber and interface properties, while the right hand sides contain terms that pertain to matrix properties, all of which are measurable physical properties. This observation emphasizes the usefulness of Eq. (24.1) to aid in the fiber, matrix and interface selection or tailoring process, in arriving at viable compositions of ECCs. As example, this approach has been adopted in the tailoring of the surface coating on PVA fibers (Li et al, 2002), and for deliberate introduction of matrix defects in lightweight ECC (Wang and Li, 2003) and high early strength ECC (Wang and Li, 2006a).

The equality signs in Eq. (24.1) are based on the assumption that initial defect size and fiber volume fraction are uniform throughout the composite. In reality, variability of these parameters must exist and depends on the mix composition as well as mixing procedure. This variability creates the need for a wider margin between the left and right hand sides in Eq. (24.1) and explains the use of the inequality signs. Kanda and Li (2006) specifically studied the necessary margin to create robust tensile properties.

24.2.4 Compressive and Flexural Characteristics

The compressive properties of ECC are not significantly different from normal to high strength concrete. Compressive strength of ECC ranges from 30MPa to 90MPa. With an elastic modulus (around 20-25 GPa) typically lower than concrete due to the absence of coarse aggregates. The compressive strain capacity of ECC is slightly higher, around 0.45-0.65%. Figure 24.5a shows a strength development curve of an ECC (M45) compressive cylinder.

The post-peak behavior of ECC under compression tends to descend more gently than high strength concrete, accompanied by a gradual bulging of the specimen (Figure 24.5b) rather than explosive crushing failure.

The flexural response of ECC reflects its tensile ductility (Maalej and Li, 1994; Wang, 2005, Wang and Li, 2006; Kunieda and Rokugo, 2006a). Under bending, multiple microcracking forms at the base of the beam allowing it to undergo a large curvature development – a phenomenon that has resulted in the popular name of “bendable concrete.” A flexural strength (modulus of rupture or MOR) of 10-15 MPa is easily achievable and accompanied by a large extent of deflection hardening regime (Figure 24.6a). Deflection hardening is an intrinsic property of ECC and does not depend on geometry. This is not the case for tension-softening FRC for which deflection hardening becomes more difficult to attain as beam height increases (Stang and Li, 2005). A highly deformed ECC beam and fine multiple cracking on the tensile side of the beam are shown in Figures 24.6b and 24.6c (Wang, 2005; Wang and Li, 2006b).

ECC has significant improvements in fatigue response over normal concrete and FRC. Suthiwarapirak et al (2002) conducted flexural fatigue test on ECC and demonstrated higher ductility and fatigue life compared with polymer cement mortars commonly used in repair applications.

24.3 Mixture Proportioning, Material Processing and Quality Control

Table 24.2 gives a typical mix design of ECC (ECC-M45) with self-consolidating casting properties. All proportions are given with materials in the dry state. The ingredients and

mix proportions have been optimized to satisfy the multiple cracking criteria Eq. (24.1). Specifically, the type, size and amount of fiber and matrix ingredients, along with interface characteristics are tailored for multiple cracking and controlled crack width. ECC incorporates fine silica sand with a sand to binder ratio (S/B) of 0.36 to maintain adequate stiffness and volume stability. ECC-M45 has a water to binder (w/b) ratio of 0.26 to attain a good balance of fresh and hardened properties. The binder system is defined as the total amount of cementitious material, i.e. cement and fly ash (Type F) in ECC. The silica sand has a maximum grain size of 250 μm and a mean size of 110 μm . Aggregated particle size of all matrix components should be properly graded to achieve self-consolidating fresh properties (Fischer et al, 2003).

Table 24.2. ECC Mix Design Proportions by Weight for ECC-M45

Mix Designation	Cement	Fly Ash	Sand	Water	HRWR*	Fiber (Vol %)
M45	1.0	1.2	0.8	0.56	0.012	0.02

*High Range Water Reducer

While various fiber types have been used in the production of ECC, ECC M45 which currently has the largest experimental dataset, uses poly-vinyl-alcohol (PVA) fiber 12 mm in length and 39 μm in diameter. The nominal tensile strength, stiffness and density of the fiber are 1600 MPa, 40 GPa and 1300 kg/m^3 , respectively. The PVA fiber is surface-coated by a proprietary oiling agent (1.2% by weight) to reduce the fiber/matrix interfacial bonding. To account for material heterogeneity, a fiber content of 2% by volume, which is greater than the calculated critical fiber content needed to achieve strain-hardening, is typically used in the mix design. The mix design described above has been experimentally demonstrated in a broad range of investigations to consistently produce good ECC fresh and hardened properties.

A high range water reducing admixture containing a polycarboxylate chemical composition has been found to be most effective in maintaining the desired fresh property during mixing and placing.

Adaptations of this reference mix have been used in various construction projects. Full-scale production of ECC was carried out in Japan (Kunieda and Rokugo, 2006b), and in the US (Lepech and Li 2007). Experience in concrete ready-mix plants suggests the following charging sequence of raw material:

Table 24.3: Material charging sequence into ready-mix trucks

Activity No.	Activity	Elapsed Time (min)
1	Charge all sand	2
2	Charge approximately 90-95% of mixing water, all HRWR, all hydration stabilizer	2
3	Charge all fly ash	2
4	Charge all cement	2
5	Charge remaining mixing water to wash drum fins	4
6	Mix at high RPM for 5 minutes or until material is homogenous	5
7	Charge fibers	2
8	Mix at high RPM for 5 minutes or until material is homogenous	5
Total		24

The properly mixed ECC material should have a creamy texture, as shown in Figure 24.7. To ensure good self-consolidation behavior, the deformability of ECC in the fresh state should be checked at the construction site. To perform this check, a standard concrete slump cone is filled with fresh ECC material and emptied onto a level Plexiglas or glass plate. The flowable ECC material flattens into a large pancake-shaped mass (Figure 24.8a). Two orthogonal diameters of this “pancake” are measured and a characteristic deformability factor, denoted by Γ , is calculated (Eqn. 2).

$$\Gamma = \frac{(D_1 - D_0)}{D_0} \quad (2)$$

where D_1 is the average of two orthogonal diameter measurements after slump cone removal, and D_0 is the diameter of the bottom of the slump cone. For good self-consolidation, Γ should have a minimum value of 2.75 (Lepech and Li, 2007). Excessively large values of Γ , however, may indicate improper mix proportions and may potentially result in component segregation, and must be avoided. Typically, the deformability value decreases over time during mixing and transport in the ready-mix concrete truck. The use of a hydration stabilizer has been found effective in maintaining good deformability without negatively affecting the hardened properties.

Care must be taken to ensure good fiber dispersion in the mix. Yang et al (2007) found that an effective means of controlling fiber dispersion is to ensure good mortar viscosity via a Marsh flow cone test. In the Marsh cone flow test, the funnel is filled completely with mortar (ECC mortar without fibers) and the bottom outlet is then opened, allowing the mortar to flow (Figure 24.8b). The Marsh cone flow time of mortar is the elapsed time in seconds between the opening of the bottom outlet and the time when light becomes visible at the bottom, when observed from the top.

To minimize the danger of early age cracking, wet curing for a minimum of two days and night pouring of field applications is recommended for ECC.

In addition to standard compression cylinder test typically applied to concrete quality control on job sites, tensile coupon test should also be carried out to assure that the tensile properties specified in design documents are met. These compression and tensile tests should be carried out at an age of 4 days, 7 days, 14 days, and 28 days to observe

property development over time. It is recognized that uniaxial tension tests are difficult to carry out on a routine quality control basis. As a result, a simpler bending test accompanied by inversion schemes to obtain material tensile properties is being developed (e.g. Kanakubo, 2006; Qian and Li, 2007).

Apart from ready-mix and self-consolidating casting, special versions of ECC have also been developed for extrusion (Stang and Li 1999), and shotcreting (Kanda et al. 2001; Kim et al. 2003; Kojima et al, 2004). Precasting of ECC structural elements has been carried out for coupling beams in highrise buildings in Japan (Kanda et al, 2006a,b). Kanda et al concluded that full-scale production in a precast plant of ECC with high mechanical performance and excellent fluidity is achievable in practice. Figure 24.9 shows the various methods of ECC material processing. While these ECC materials all carry the same hardened material characteristics described in Section 24.2, they exhibit significantly different fresh properties to meet different processing requirements. The relatively small amount of fibers used in ECC enables such versatility in processing methods.

24.4 Behavior of ECC Structural Elements

A variety of experiment programs have been performed to assess the performance of ECC at the structural element level for both seismic and non-seismic structural applications (Table 24.4). These experiments provide insight into how unique ECC material properties elevate the response performance of the structure. Within this section, we describe some observed responses of elements subjected to monotonic and fatigue flexural loading, cyclic shear loading, and steel-ECC interactions. Fundamental knowledge will then be drawn from these studies.

Table 24.4: A summary of various R/ECC structural elements previously studied

Structural Element Type	Type of Loading (type of reinforcement)*	Reference
Flexural elements	Reversed cyclic Monotonic (GFRP) Reversed cyclic (CFRP) Fatigue	Fischer & Li, 2002 Li & Wang, 2002 Fischer & Li, 2003a Kim et al, 2004
Column elements	Reversed cyclic	Fukuyama et al, 2000
Shear beam elements	Reversed cyclic Reversed cyclic Monotonic Monotonic	Kanda et al, 1998 Fukuyama et al, 2000 Shimizu et al, 2006 Kabele & Kanakubo, 2007
Beam-Column connections	Reversed cyclic	Parra-Montesinos & Wight, 2000
Wall elements	Repeated shear Reversed cyclic Reversed cyclic	Kanda et al, 1998 Kesner & Billington, 2005 Fukuyama et al, 2006
Frames	Reversed cyclic (steel and	Fischer & Li, 2003b

	CFRP)	
Steel/ECC interactions	Monotonic flexure (plate/ECC) Monotonic shear (stud/ECC) Monotonic tension (anchor/ECC)	Walter et al, 2004 Qian and Li, 2006 Leung, C.K.Y. et al, 2006 Qian, 2007

* steel reinforcement unless specified

24.4.1 Structural Response of R/ECC Elements

24.4.1.1 Flexural Elements

Fischer and Li (2002) studied the behavior of R/ECC flexural elements under reversed cyclic loading. The test set up is shown in Figure 24.10, and the specimen configuration is shown in Figure 24.11. A regular R/C beam was also tested as control. Figure 24.12 shows the substantial difference in hysteretic response for the R/ECC and the R/C control column specimens. A significantly fuller hysteretic loop with larger energy dissipation was achieved by the R/ECC beam despite the fact that no shear stirrups were used at the base of the flexural element. The damage experienced by these elements at 10% interstory drift is compared in Figure 24.13. Even at this high drift level, no spalling of the ECC was observed. In contrast, the R/C column lost all concrete cover near the fixed end subsequent to bond splitting and spalling. Clearly, the R/ECC element demonstrated significant damage tolerance under severe loading.

High cycle fatigue response of R/ECC flexural elements was studied by Kim et al (2004) in conjunction with a bridge deck link slab application. The full thickness slab test configuration is shown in Figure 24.14 with the steel girder (anchored to the slab by steel studs) on top for convenience of testing. Over 100,000 cycles, no degradation in stiffness was observed in the R/ECC or in the R/C control beam. However, the cracks in the R/C beam grew continuously to 0.6 mm at the end of the test, while the microcracks in R/ECC beam remained at approximately 50 μm (Figure 24.15).

Motivated by the need to increase the stiffness and to reduce the tendency for fatigue cracking in steel bridge decks, a steel/ECC composite beam was studied by Walter et al (2004) under monotonic flexural loading (Figure 24.16). For control, a steel/FRC and a steel/FRD composite beam were also tested in the same configuration. FRD is a fiber reinforced Densit material, a very high strength and dense concrete reinforced with steel fibers similar to Ductal. All concrete materials were cast onto the steel plate and bonded only by adhesion to the roughened steel surface. The load-deflection response captured in Figure 24.17 demonstrates a much higher load capacity in the case of the steel/ECC beam which showed multiple microcracking during testing, suppressing the formation of a brittle fracture that limits the capacity of the steel/concrete beam. The single fracture in the FRC and FRD beams led to their immediate debonding from the steel plate.

24.4.1.2 Shear Element

Fukuyama et al (2000) studied the behavior of R/ECC shear elements under reversed cyclic loading. The specimen configuration is shown in Figure 24.18 while the hysteretic loops for R/ECC and R/C are shown in Figure 24.19. Again, the hysteretic loops for R/ECC showed much greater stability and ability to dissipate energy. The R/C specimen suffered extensive bond splitting and loss of cover, accompanied by large diagonal cracks. In contrast, the damage experienced by the R/ECC shear element was significantly lower (Figure 24.20). No bond splitting and cover loss was observed and microcracks continued to carry loads up to 5% rad deflection angle.

The shear capacity of a R/ECC beam can be estimated from a linear superposition of the contributions of the ECC material and the shear and axial steel reinforcements due to the compatible deformation of the two materials even after steel yields. This approach was suggested to be reasonably accurate and conservative (Rokugo et al, 2007). However, numerical analysis combined with experimental data (Kabele and Kanakubo, 2007) suggested that only a fraction of the ECC's tensile strength and strain capacity might be utilized in shear element due to possible damage of bridging fibers on sliding crack surfaces.

24.4.1.3 Column Element

The response of R/ECC and R/C columns under fully reversed cyclic loading was studied by Fukuyama et al (2000). These columns were tested under anti-symmetrical moment condition. The axial force applied to the column is 20% of the axial compressive strength of the column, calculated without the contribution of the steel reinforcements. The hysteretic behavior in terms of stability and energy dissipation was improved in R/ECC column over R/C column in a similar manner as for flexural and shear elements (Figure 24.21). Large bond splitting cracks were observed in the R/C column which failed by shear without yielding of the longitudinal reinforcements. Subsequently, the resistant shear force in the envelope curve of shear force – deflection angle relationship decreased with increase of deflection angle. On the other hand, the R/ECC column did not fail by shear or bond splitting. Instead, it maintained a ductile response up to the end of the test with fine cracks revealed on the specimen surface.

24.4.1.4 Beam-Column Connection Element

Beam-column connection was studied by Parra-Montesinos and Wight (2000), with the test set up shown in Figure 24.22. The hysteretic response for the R/ECC shear panel was substantially improved over the R/C (Figure 24.23), even when all shear stirrups were removed in the R/ECC shear panel. Under fully reversed cyclic loading, a set of orthogonal cracks formed in both specimens (Figure 24.24). While the orthogonal cracks in R/ECC were much more closely spaced, they did not lead to surface spalling as often observed in R/C specimens after large load reversals. In addition, edge spalling was revealed in the R/C specimen, associated with the bearing of the steel beam on the brittle concrete. This was not found in the R/ECC specimen.

24.4.1.5 Wall Panel Element

Wall panel elements were studied by Kesner and Billington (2005) under fully reversed cyclic loading, with the test set up shown in Figure 24.25. These tests confirmed that the R/ECC wall panels outperformed the R/C wall panels in hysteretic loop stability, peak load, and energy dissipation (Figure 24.26).

The structural element experimental testing results briefly summarized above share the common features of enhanced element load and deformation capacity, hysteretic loop stability, and energy dissipation. Further, structural damage is limited to microcracking while large fractures in the form of bond splitting and spalling are suppressed.

24.4.2 Insights from R/ECC element response

A number of helpful insights for structural use of ECC can be drawn from the above studies. These are summarized below.

24.4.2.1 Potential for reduction or elimination of shear reinforcement

Through the formation of multiple cracks and delay of fracture localization, the ductility of R/ECC elements can be maintained with little or no conventional shear reinforcement. This is best demonstrated in the flexural element (Fischer and Li, 2002a, Figure 24.11) and the beam-column connection (Parra-Montesinos and Wight, 2000) studies highlighted in the previous section, where shear stirrups were completely eliminated. Additional evidence can be found in a study by Li and Wang (2002) who experimentally demonstrated that ECC beams without shear reinforcement exhibited superior performance to high strength concrete beams with closely spaced steel stirrups. Experiments on the cyclic response of unbonded post-tensioned precast columns with ECC hinge zones (Billington and Yoon, 2004) also confirmed that the column integrity could be better maintained when concrete is replaced by ECC without any seismic shear detailing.

24.4.2.2 Damage tolerance

Damage tolerance is a measure of the residual strength of a material or structure when damage is introduced. The damage tolerance of ECC derives from the fact that fracture or real cracks are suppressed in favor of “plastic yielding” of ECC in the form of multiple microcracks. Such microcracks are not real cracks (Li, 2000) in the sense that an increasing amount of load can be carried across them during ECC strain-hardening. Cracks in normal concrete or even in standard fiber reinforced concrete are accompanied by tension softening and load carrying capacity drops as the crack enlarges. As a result, a reliance on steel reinforcement to maintain structural integrity becomes critical. Where no steel reinforcement exists, e.g. in the concrete cover, surface spalling results. Such failure modes are fully eliminated in R/ECC elements, as can be observed in Figures 24.13, 24.20, and 24.24. In these elements, the shear stiffness and the peak load at each load cycle is better maintained than in R/C through ECC’s high damage tolerance capability. In structural elements loaded beyond first crack, it is reasonable to expect equal or even higher structural stiffness in R/ECC elements compared to R/C elements,

despite the lower elastic modulus of ECC as compared to concrete. This is due to the capability of ECC to continue to share the load carrying function with steel reinforcements, long after the first crack appears. This concept was verified in an analytic study of cracked reinforced beams by Szerszen et al (2006).

Fukuyama et al (2007) regarded such damage tolerance functionality of ECC as a significant benefit to society given the enormous economic cost of repair and reconstruction of infrastructures after a major seismic event that strikes an urban area.

24.4.2.3 Compatible deformation between ECC and reinforcement

In R/ECC members with steel reinforcement, both the steel and the ECC can be considered elastic-plastic materials capable of sustaining deformation up to several percent strain. As a result, the two materials remain compatible in deformation even as both steel and ECC “yield”. Compatible deformation implies that there is no shear lag between the steel and the ECC, resulting in a very low level of shear stress at the steel rebar to ECC material interface. This phenomenon is unique to R/ECC members. As a result of this low interfacial stress between steel and ECC, the bond between ECC and reinforcement is not as critical as in normal R/C elements, since stress can be transmitted directly through the ECC material (via bridging fibers) even after microcracking. In contrast, within R/C members stress must be transferred via the rebar-concrete interface to the concrete away from the crack site. After concrete cracks in an R/C element, the concrete unloads elastically near the crack site, while the steel takes over the additional load shed by the concrete. This leads to incompatible deformation and high interface shear stress responsible for the commonly observed failure modes such as bond splitting and/or spalling of concrete cover. Figure 24.27a shows the stress flow in the composite before and after matrix cracking, in R/C and R/ECC. The compatible deformation between ECC and reinforcement has been experimentally confirmed (Fischer and Li 2002b). Figure 24.27b shows the contrasting behavior of R/ECC and R/C near the interface, revealed in a cross-sectional cut of tension-stiffening specimens.

In structural elements subjected to large loads such as earthquakes, steel yielding may be expected. In R/C elements, steel yielding may be concentrated at locations where the rebar crosses the concrete cracks due to the large incompatible deformations between the steel and fractured concrete. In R/ECC elements, steel yielding can spread to a much larger area. As a result, the distributed microcracking in ECC allows for more efficient utilization of steel reinforcement for element energy dissipation. This explains the formation of fuller hysteretic loops observed in the ECC elements discussed in Section 24.4.1 (Figures 24.12, 24.19, 24.21, 24.23, 24.26).

24.4.2.4 Tight crack width control and elimination of crack control reinforcement

A common observation in the structural element tests described is that the cracks generated in the R/ECC have very small crack widths (Figures 24.13, 24.15, 24.20, 24.24). This is because crack widths in ECC are self-controlled (Section 24.2.2). While the presence of steel reinforcement further limits the crack width, ECC material can be easily designed to have crack width less than 100 μm without depending on steel reinforcement. This small crack width is important with respect to durability of the

structure (Section 24.5), and can be decisive in determining whether a structure requires repair after a major loading event (Fukuyama et al, 2007).

24.4.2.5 Transforming material ductility into structural strength

Once again, the unique feature of ECC is its ultra high ductility. This implies that structural failure by fracture is significantly less likely in comparison to normal concrete or FRC.

In traditional R/C structural design, the most common and most important material parameter of concrete is compressive strength. For this reason, structural strength (and more generally, structural performance) is often perceived to be governed by material strength. Essentially, higher material strength (usually referred to compressive strength in the concrete literature) is expected to lead to higher structural strength. This concept is valid only if the material strength property truly governs the failure mode. However, if tensile fracture failure occurs, a high strength material does not necessarily mean higher structural strength. Rather, a high toughness material, and in the extreme, a ductile material like ECC, can lead to a higher structural strength.

A number of recent experimental observations (Lim and Li 1997; Kanda et al. 1998; Fukuyama et al, 2000; Kesner and Billington 2005) provide support for the above reasoning. For example, the shear beam elements tested by Fukuyama et al (Figure 24.18) have compressive strengths of 58.3 MPa and 52.5 MPa for concrete and ECC, respectively. However, the structural load capacity was 120 kN versus 140 kN for the R/C and R/ECC elements, respectively (Figure 24.19). As another example, the precast in-fill wall panels (Figure 24.25) tested by Kesner and Billington for seismic retrofitting of buildings revealed that a panel with a concrete of compressive strength of 50 MPa attained a structural (shear) strength of 38 kN, while a similar panel made with ECC material of lower compressive strength (41 MPa) achieved a much higher structural strength of 56 kN (Figure 24.26). The over 35% structural strength gain in the R/ECC panel can be attributed to material ductility of the ECC that prolonged integrity of the panel to a larger drift level. Similarly, detailed numerical analysis (Kabele, 2001) of a wall panel made with ECC demonstrated a structural strength three times that of the panel made with FRC, despite the fact that both materials had the same tensile and compressive strengths.

24.5 Durability of ECC and ECC Structural Elements

24.5.1 Material and Element Durability

As a new construction material, it is not enough to have excellent mechanical performance compared with conventional concrete or FRC. It is important also to verify the durability of the ECC material itself in various environments typical of where such materials are expected to be used. In addition, the influence of this material on structural durability performance of R/ECC must also be confirmed. In most cases, laboratory studies are performed under accelerated conditions. However, long-term performance in

the field is most valuable even though this is difficult to obtain, especially for a relatively new material.

Since the greatest value of ECC lies in its superior tensile ductility, this material will likely be used in structures that impose large deformations on the material. This implies that the structure must remain serviceable even if the material undergoes tensile strain hardening accompanied by multiple microcracking. For this reason, the examination of ECC material durability should be carried out in the deformed cracked state. That is, the ECC specimen should undergo preloading to varying strain levels, in order to deliberately create microcrack damage, prior to accelerated exposure tests. Experimental data thus determined from preloaded specimens may be considered as material durability properties under combined mechanical and environmental load. It should be noted, however, that most of these experiments were undertaken with cracked specimens in the unloaded state for experimental testing convenience. On unloading, crack widths in ECC tend to reduce by 10-20% from the loaded state. This reduced crack width is used in all experimental data reported. This difference from field conditions where cracks are typically under load is not expected to have a significant impact on the measured durability of ECC material or R/ECC structures, but should be verified in future studies.

As will become clear in the following subsections, the durability of ECC and especially of ECC structures can be sensitive to the width of the microcracks. Fortunately, microcrack widths are designed to be small, typically less than 100 μm for ECC, and potentially much lower. These cracks remain small under fatigue loading, as indicated in Section 24.4.1.1. However, a recent study by Boshoff and van Zijl (2007) indicates that crack width may open wider under sustained loading due to creep mechanisms. Care must be taken for the long-term durability of a structure under combined conditions of sustained loading, deformation to the strain-hardening stage and exposure to an aggressive environment.

In Section 24.5.2, current knowledge of ECC durability under various environments is summarized. In Section 24.5.3, the durability of R/ECC under chloride exposure is presented. This is followed (Section 24.5.4) by highlights of limited long-term performance data on ECC materials already in structures exposed to the natural environment and (in one case) also in combination with mechanical loads. Additional studies of ECC under various environmental and/or loading conditions can be found in the references in Table 24.5.

Most of the durability studies covered here are for ECC reinforced with PVA fibers. The durability of PVA fiber itself has been summarized by Horikoshi et al (2006).

Table 24.5: Studies of ECC durability under various environments/loading conditions

Environments/loading conditions	References
Long term aging	Li & Lepech, 2004
Freeze-thaw cycles	Li et al, 2003
Tropical climate exposure	Li et al, 2004

Chloride immersion	Li et al, 2007
Deicing salt exposure	Şahmaran & Li, 2007a
Alkali-silicate reaction	Şahmaran & Li, 2007b
Fatigue	Suthiwarapirak et al, 2002
Creep under constant load	Boshoff, & van Zijl, 2007
Wheel load abrasion	Li & Lepech, 2004
Restrained drying shrinkage	Li and Stang, 2005 Wang and Li, 2006
Calcium leaching	Nemecek et al, 2006

24.5.2 ECC Durability Under Various Environments

In this section, current knowledge on long-term strain capacity, as well as ECC exposed to various commonly encountered environments is summarized. These environments include freeze-thaw cycles, hot-wet cycles, chloride immersion, deicing salt exposure, and alkali-silicate reaction (ASR) resistance.

24.5.2.1 Long Term Tensile Strain Capacity

For a construction material to be considered truly durable, its mechanical properties must not degrade over time and falling below minimum design specifications. To validate ECC long-term effectiveness, a series of tensile tests were performed to determine long-term strain capacity. Due to the continued hydration process typical of cementitious materials, and the delicate balance of cement matrix, fiber, and matrix/fiber interface properties in ECC, the strain capacity of ECC evolves with age during maturing (Li and Lepech, 2004). This is exhibited in a plot of ECC strain capacity versus age (Figure 24.28). Roughly 10 days after casting, peak strain capacity is achieved when an optimal balance of matrix, fiber, and matrix/fiber interface properties is attained for highly saturated multiple cracking. As hydration continues, the increasing matrix toughness leads to a reduced composite ductility. Maturity of matrix and fiber/matrix properties eventually results in an ECC long-term steady strain capacity of 3%, far above the deformation demand imposed by many structural applications, but significantly less than the 5% capacity seen at early age. While long-term tests have only been carried out to 180 days, the long-term strain capacity is expected to remain at approximately 3%.

The strain capacity–age curve can be seen as analogous to the compressive strength development curve in normal concrete. However, because it is not monotonically rising, the long-term value should be used for design purposes. For simplicity, 90% of the 28-day strain-capacity value that approaches asymptotically to the long-term behavior may be adopted as the design strain-capacity. This makes it easy for design as the same 28-day value is used for compressive strength specification.

24.5.2.2 Freeze Thaw Durability

Durability of non-air-entrained ECC specimens was tested by exposure to cycles of freezing and thawing, in accordance with ASTM C666. Non-air-entrained concrete specimens were also tested as reference specimens. Testing of ECC and concrete prism

specimens was conducted concurrently over 14 weeks (Li et al, 2003). After 5 weeks (110 cycles), the concrete specimens had severely deteriorated, requiring removal from the freeze-thaw machine, as mandated by the testing standard. However, all ECC specimens survived the test duration of 300 cycles with no degradation of dynamic modulus (Figure 24.29). This performance results in a durability factor of 10 for concrete compared to 100 for ECC, as computed according to ASTM C666. In uniaxial tension tests performed on wet cured and freeze thaw exposed ECC tensile coupons at the same age, no significant drop in strain capacity is experienced after 300 cycles. Both wet cured and freeze thaw specimens exhibit a strain capacity of roughly 3%.

24.5.2.3 Tropical Climate Exposure

In contrast to freeze thaw tests discussed above, which are designed to simulate temperature changes in winter conditions, hot water immersion tests were conducted to simulate the long term effects of hot and humid environments. To examine the effects of environmental exposure, hot water immersion was performed on individual fibers, single fibers embedded in ECC matrix, and composite ECC material specimens (Li et al, 2004). Specimens for both individual fiber pullout and composite ECC material were cured for 28 days at room temperature prior to immersion in hot water at 60°C for up to 26 weeks. After this exposure, little change was seen in fiber properties such as fiber strength, fiber elastic modulus, and elongation. However, the strain capacity of the ECC did drop from 4.5% at early age to 2.75%. While accelerated hot weather testing result in lower strain capacity of ECC, the 2.75% strain capacity, over 250 times that of normal concrete, seen after 26 weeks and equivalent to 70 years of natural weathering (Proctor et al, 1982), remains acceptable for most infrastructure applications.

24.5.2.4 Chloride Immersion

When ECC material is exposed to environments with high chloride concentrations, such as marine structures or for pavements and bridge decks subjected to de-icing salt applications, chloride ions may alter the fiber/matrix interface and therefore the composite properties. To examine these effects, ECC coupon specimens were first preloaded under uniaxial tension to different strain levels, then exposed to a 3% NaCl solution at room temperature for 1, 2 and 3 months and then subsequently reloaded up to failure (Li et al, 2007). Figure 24.30 shows the data for the three sets of specimens preloaded to 0 (virgin), 0.5% and 1.5% tensile strain. In all cases, the reloaded specimens retained multiple micro-cracking behavior and tensile strain capacity of more than 3%, although the average crack width increased from 40µm to 100µm and the tensile strength was reduced by about 10%. The wider crack width and lower tensile strength may be a result of a reduction in chemical bonding at the fiber/matrix interface, as suggested by single fiber pull-out test data by Kabele et al (2007).

24.5.2.5 Deicing Salt Exposure

Şahmaran and Li (2007a) studied the durability performance of non-air-entrained ECC when subjected to mechanical loading and freezing and thawing cycles in the presence of de-icing salts. After 50 exposure cycles, the surface condition visual rating and total mass of the scaling residue of ECC remained within acceptable limits according to ASTM C 672 (Figure 24.31a). This level of durability held true even for specimens pre-

loaded to cracking at high deformation levels. Non-air-entrained mortar specimens were used as reference specimens. As expected, these mortar prisms under identical testing conditions deteriorated severely. Pre-loaded and virgin (no pre-loading) ECC coupon specimens were also exposed to freezing and thawing cycles in the presence of de-icing salts for 25 and 50 cycles to determine their residual tensile behavior. The reloaded specimens showed negligible loss of ductility, but retained multiple micro-cracking behavior and a tensile strain capacity of more than 3% (Figure 24.31b). It was also found that multiple micro-cracks due to mechanical loading healed sufficiently under freezing and thawing cycles in the presence of salt solutions and restored the specimens to nearly the original stiffness. These results confirm that ECC, both virgin and micro-cracked, remains durable despite exposure to freezing and thawing cycles in the presence of de-icing salts.

24.5.2.6 Alkali-silicate Reaction Resistance

Şahmaran and Li (2007b) studied ECC's resistance to alkali-silicate reaction (ASR). ECC bar specimens were immersed in alkali solution at 80°C in accordance to ASTM C 1260 to determine their length change due to alkali silica reaction. The ECC bar specimens containing either Class F or Class C fly ash did not show any significant expansion at the end of a 30-day soaking period (Figure 24.32). Although very fine silica sand is used in ECC, the crystalline nature of these sand particles suppresses the reactivity in an alkaline environment. Further, the presence of a high volume of fly ash decreases the pH value due to the pozzolanic reaction, making alkali-silicate reaction even less likely. Finally, the presence of the PVA microfibers tends to reduce any expansion that may occur. These studies show that ECC material will not exhibit degradation due to ASR.

24.5.3 Durability of R/ECC

Increased durability of reinforced concrete is typically associated with a dense concrete matrix, that is, a very compact microstructure expected to lower permeability and reduce transport of corrosives to the steel (Beeldens and Vandewalle, 2001; Oh et al, 2002). This can be achieved with a well-graded particle size distribution, fly ash and silica fume, or low w/c ratios. These concepts, however, rely upon the concrete to remain uncracked within a structure throughout its expected service life and resist the transport of water, chloride ions, oxygen, etc. In this presumed uncracked state, numerous concrete materials have shown promising durability in laboratory tests (Mora et al, 2003; Weiss and Shah, 2002).

In reality, however, reinforced concrete members crack due to applied structural loads, shrinkage, chemical attack and thermal deformations, which are practically inevitable and often anticipated in restrained conditions (Mihashi and De Leite, 2004; Wittmann, 2002). The durability of concrete is intimately related to its transport properties, that is, the rate at which corrosives and water are able to penetrate the concrete. This is because concrete is susceptible to degradation through leeching, corrosion, sulfate attack, freezing-and-thawing damage, and other mechanisms that depends on the ingress of water. Because cracks significantly modify the transport properties of concrete, their presence greatly

accelerates the deterioration process. To solve this serious problem, a fundamental solution that reduces the brittle nature of concrete is needed.

The use of ECC to replace normal concrete in steel reinforced concrete structures has a number of implications in terms of structural durability. These implications include

- a) Alteration of transport properties in the concrete or “ECC” cover, thereby delaying the reach of aggressive agents to steel reinforcements, through the intrinsic tight crack width control of ECC,
- b) Alteration of the nature of steel corrosion with potentials for avoiding pitting and slowing the rate of corrosion, through dispersed microcracking over a region of the steel reinforcement rather than concentrating at the base of a large crack, and by its resistance to cover spalling via ECC’s tensile ductility.

These two alterations lead to expected improvements in structural durability through delay of steel corrosion initiation phase, and once initiated, dramatically slow the steel corrosion propagation phase. A number of experimental research efforts have been conducted which focus on the transport properties of ECC, especially when it is already in the strain-hardening stage with the presence of multiple microcracks, and on the behavior of steel reinforced ECC elements in accelerated testing environments. Major findings of these two aspects are summarized in the following subsections.

Recommendations for serviceability design of R/ECC structures against carbonation and chloride ion induced steel corrosion can be found in Rokugo et al (2007).

24.5.3.1 Transport Properties of ECC

The most important transport properties of ECC include

- a) Permeation in the presence of a hydraulic pressure, such as the condition in liquid containers and reservoir dams,
- b) Diffusion in the presence of a ion concentration gradient, such as the condition on bridge decks, salt tanks and marine environments, and
- c) Capillary suction induced by surface tension, of particular importance in ECC when crack width becomes very tight.

All transport property tests described below were conducted at 28 days of age.

24.5.3.1.1 Water permeation

Lepech and Li (2005) found that cracked ECC exhibited nearly the same water permeability ($k \sim 5 \times 10^{-11}$ m/s) as sound concrete, even when strained in tension to several percent (Figure 24.33). Within this study, both ECC and reinforced mortar specimens were pre-tensioned up to 1.5% deformation, resulting in a variety of crack widths and number of cracks among the various specimens. The permeability of these cracked materials was then determined under a hydraulic head. As seen, there was dramatic rise in permeability with increasing crack width. For the ECC specimens, the crack width was intrinsically limited to about 60 μm (Section 24.2.2), regardless of the tensile deformation imposed. Thus, the measured permeability was correspondingly low.

Further, when normalized by number of cracks within the specimen, the comparable permeability of cracked ECC with sound material became even more apparent.

24.5.3.1.2 Chloride diffusion

Chloride diffusion coefficients for ECC were examined by Şahmaran et al (2007). Beam specimens were ponded in saltwater solution with 3% NaCl, according to AASHTO T259-80. These measured values should really be regarded as “effective chloride diffusion coefficient” since the actual transport process is likely more complex than diffusion in a homogeneous medium without cracks. Based on tests on uncracked beams, the chloride diffusion coefficient for ECC was found to be 6.75×10^{-12} m²/s, compared with 10.58×10^{-12} m²/s based on tests on steel reinforced mortar beam used as a control. Under high imposed bending deformation, preloaded ECC beam specimens revealed microcracks less than 50 µm and an effective diffusion coefficient significantly lower than that of similarly preloaded reinforced mortar control beams due to the tight crack widths inherent in ECC. In contrast, cracks larger than 150 µm were often produced under the same imposed deformation levels for the reinforced mortar beams. Figure 24.34 shows the measured effective diffusion coefficient versus pre-loading deformation level for ECC and mortar. It is revealed that the diffusion coefficient of ECC varies linearly with the number of cracks (with crack width intrinsically constant even as beam deformation increases), whereas the diffusion coefficient of reinforced mortar is proportional to the square of the crack width.

Chloride diffusion was also studied by Oh and Shin (2006) for specimens subjected up to 100,000 cycles of flexural loading. They found that the chloride diffusion coefficient did not increase significantly despite the increase number of cracks, and attribute this finding to the very fine crack width.

24.5.3.1.3 Capillary Suction

Şahmaran and Li (2007c) analyzed the water absorption and sorptivity properties of preloaded ECC, based on ASTM C642 and ASTM C1585 test procedures. Water absorption testing measures the mass of absorbed water per unit mass of the pre-dried concrete material, after complete immersion in water until saturation is reached. Water absorption is expressed in terms of the volume percent of permeable pores. The sorptivity test measured the increase in mass of a pre-dried specimens at given intervals of time when permitted to absorb water by capillary suction in one direction, and is quantified by the sorptivity index.

The findings of Şahmaran and Li, which emphasized the impacts of the presence of (a) microcracking and (b) water repellent admixture, on water absorption and sorptivity, are summarized in Figure 24.35. From this figure, it can be seen that the presence of microcracks in ECC composites without water repellent admixtures can lead to an exponential increase of the sorptivity index with the number of microcracks. However, sorptivity index values of cracked ECC are not particularly high when compared with that of normal concrete, probably due to the higher amount of cementitious materials, lower water-cementitious materials ratio and high volume fly ash content. For the ECC mixture with water repellent admixture, the presence of microcracks and their number

had little or no effect on the sorptivity index. The water repellent agent based on water soluble silicon was very effective in reducing the sorptivity index of cracked ECC. ECC mixtures with water repellent admixtures also showed lower percentages of permeable pores compared to the ECC mixtures without water repellent admixture. In contrast to the sorptivity index, there was no significant influence of the number of cracks on the volume of permeable pores among the same ECC mixtures.

According to Neville (1995), typical sorptivity index is $0.09 \text{ mm/min}^{1/2}$ for normal concrete with a w/c ratio of 0.4. Some other research studies suggested that ordinary Portland cement concrete with w/c ratio of 0.4–0.5 would have sorptivity index of about $0.23 \text{ mm/min}^{1/2}$ (e.g. Mehta and Monteiro, 2006). Therefore, the sorptivity index for these cracked and virgin ECC specimens at w/cm ratio of 0.27 (especially for those containing water repellent admixtures, at about $0.02\text{-}0.03 \text{ mm/min}^{1/2}$) was significantly lower than that of conventional concrete. Water absorption test by Mechtcherine and Lieboldt (2007) also confirmed that ECC strained to between 0.5% and 1% showed “water retardant” ability. The findings by Şahmaran and Li (2007), together with those of Mechtcherine and Lieboldt, confirm that capillary suction does not pose a danger to the durability of ECC structures despite the expected presence of fine cracks. This risk is further reduced by the use of water repellent admixtures. These conclusions are consistent with the findings of Martinola et al (2004).

24.5.3.2 Corrosion Resistance in R/ECC

From the discussions presented in Section 24.5.3.1, the transport properties of ECC associated with permeation under hydraulic gradient, diffusion under ion concentration gradient, or sorption and absorption under capillary suction, all show the tendency to improve over concrete and especially cracked concrete. Given that concrete structures are designed to allow some tensile cracking, and that these cracks within reinforced concrete are typically the source of corrosion due to the increased transport of water and corrosives, there is substantial potential for ECC to improve the durability of R/C structures by acting as a quality cover where all transport mechanisms are substantially inhibited. The interaction between ECC and steel reinforcement from the viewpoint of corrosion resistance has been examined. The nature and rate of steel corrosion in ECC, and the spall resistance of ECC when specimens are subjected to accelerated testing conditions are presented below.

24.5.3.2.1 Nature of Steel Corrosion

A study on chloride penetration rate and corrosion rate of steel reinforcement has been carried out by Miyazato and Hiraishi (2005). Preloaded R/ECC and R/C beams were exposed to 28 day chloride accelerated environment with wet (saltwater shower 90% RH – 2 days) and dry (60% RH – 5 days) cycles. They found that chloride penetration reaches 0-20 mm and 80-100 mm in the R/ECC and the R/C beams respectively. The total (macro and micro cell) steel rebar corrosion rate was measured to be less than 0.0004 mm/year in the R/ECC but exceeded 0.008 mm/year in the R/C beams (Figure 24.36).

The observed smaller chloride penetration depth is consistent with the smaller effective diffusion coefficient found by Şahmaran et al (2007) discussed in Section 24.5.3.1.2. The nature of corrosion in R/ECC is decidedly different from that in R/C. Microcell currents formed between the closely spaced microcracks in the R/ECC dominate macrocell currents so that the length of steel reinforcement that experiences corrosion is longer in the R/ECC. The much higher rebar corrosion rate concentrated at the location of the concrete crack in the R/C specimen suggests a higher tendency for pitting corrosion of the steel reinforcement to occur.

24.5.3.2.2 Corrosion Propagation and Spall Resistance

Given the tensile ductility of ECC, the ability for the cover to remain intact despite steel corrosion serves as a possibility to further prolong the service life of R/ECC structures. Şahmaran et al (2006) conducted an experimental investigation on R/ECC beams subjected to accelerated corrosion by electrochemical method, designed to induce different degrees of corrosion into the reinforcement (a single steel rebar) embedded in ECC prismatic specimens. These experiments aimed at examining the spall resistance of R/ECC cover, the influence of an intact cover on the corrosion process in the corrosion propagation phase, the rate of loss of steel by corrosion, and the residual load capacity of R/ECC elements.

Corrosion-induced crack width of mortar specimens increased with time as corrosion activity progressed. Larger crack widths, up to 2 mm wide, were obtained at higher levels of corrosion. On the other hand, crack widths of ECC remained nearly constant (~0.1 mm) with time as corrosion activity progressed, while the number of cracks on the surface of the specimen increased. The results of this study also showed that ECC has significant anti-spalling capability as compared to conventional mortar (Figure 24.37). If a crack width of 0.3 mm (as specified by AASHTO (2004) for maximum crack width limit for outdoor exposures) were used to represent the serviceability limit of reinforced concrete structures, the service life of reinforced ECC would be at least 15 times that of the reinforced mortar.

Reinforcement corrosion in mortar specimens resulted in a marked reduction in stiffness and flexural load capacity. After 25 hours of accelerated corrosion exposure, the flexural strength reduced to about 34% of the original flexural capacity of the control mortar beam. In contrast, the ECC specimens after 50 hours of accelerated corrosion exposure retained almost 100% of the original flexural capacity of the control specimens. Beyond 50 hours, the flexural capacity decreased, but retained over 45% that of the control specimens even after 300 hours of accelerated corrosion exposure. Longitudinal cracks due to expansion of the corrosion products also affected the failure mode of the reinforced mortar under four-point bend load (Figure 24.38). On the other hand, ECC deterioration due to the corrosion of reinforcement did not modify the type of failure in ECC beams.

The loss in load carrying capacity is related to the mass loss of the steel reinforcement due to corrosion. The percentage of steel mass losses within the ECC and mortar beams throughout the accelerated corrosion process is presented in Figure 24.39. The average percentage of mass loss of steel reinforcing bars embedded in the mortar specimens were 2.5%, 5.3% and 11.7% at the end of 25, 50 and 75 hours accelerated corrosion test, respectively. On the other hand, there was nearly no mass loss of steel reinforcing bars embedded in ECC specimens after up to 50 hours of accelerated corrosion testing and the average percentage of mass loss of reinforcing bars embedded in ECC was 17.5% at the end of 300 hours of accelerated corrosion testing.

The observed superior corrosion performance of ECC compared to mortar in terms of corrosion propagation time, tight crack width, lower weight loss, and higher retention of stiffness and flexural strength, is attributable to the high tensile strain capacity, strain hardening performance, and multiple-cracking behavior of ECC. Overall, the experimental results from this study suggest that the propagation period of corrosion could be safely included in estimating service life of a structure when concrete is replaced by ECC.

24.5.4 Long Term Performance

The long-term performance of ECC in full-scale structures has not been fully established given the relatively recent development of this material. However, at least two field demonstration studies provide limited data that support the contention that ECC can be durable under actual field conditions.

One study (Rokugo et al, 2005) involves the use of ECC for repair of a concrete gravity earth-retaining wall (18m in width and 5m in height) that had been damaged by alkali-silica reaction (ASR) cracking. The decision to use ECC for the 50-70 mm thick repair overlay was based on the need to prevent cracks in the substrate concrete from reflecting onto the repair layer. Such reflection was anticipated had normal concrete been used in this repair given continued ASR expansion. For demonstration, the wall was divided into 9 repair blocks with an additional block (block 10) left unrepaired. For the repaired blocks, two types of ECC, one containing 1.5% hybrid PVA and PE fibers (blocks 1-4), and another containing 2.1% PVA fibers (blocks 5-8), were applied. In each block, either welded wire mesh reinforcement, or expanded metal reinforcement, or no reinforcement was used. For control, a welded wire mesh reinforced repair mortar was applied to block 9.

Since the repair took place in 2003, this wall has been continuously monitored. No cracking in the overlay was observed until seven months after repair by ECC, while cracking was visually observed on the blocks repaired with normal mortar just one month after repair. The crack widths in the ECC repair blocks were less than 50 μm and 120 μm at 10 and 24 months, respectively. In contrast, the crack widths in the normal repair mortar block were 200 μm and 300 μm at 10 and 24 months, respectively. The crack patterns at 12 months and 24 months are shown in Figure 24.40.

Another long-term performance verification is afforded by a small ECC patch repair placed on the bridge deck of Curtis Road over M-14 in Southern Michigan in 2002, in collaboration with the Michigan Department of Transportation. A complete summary of this work has been outlined by Li and Lepech (2004). During this work, one section of a deteriorated bridge deck was repaired with ECC while the remaining portion was repaired with a commercial concrete patching material commonly used by MDOT (Figure 24.41a). This repair scenario allowed for a unique ECC/concrete comparison subjected to identical environmental and traffic loads. (This road is used frequently by 11 axle trucks heavily loaded with aggregates, although it has a relatively low averaged daily traffic of 3000 vehicles/day). The concrete repair material used was a pre-packaged mixture of Portland cement and plaster of paris. At this writing, the repaired bridge deck has experienced more than six complete Michigan winter cycles of freezing and thawing, in addition to live loads. The monitored crack width development is shown in Figure 24.41b. While the ECC patch repair has survived this combined loading state with minor microcracking limited to less than 50 μm , the concrete repair portion experienced cracking in excess of 3.5 mm and had to be re-repaired in 2005.

24.6 Concluding Remarks

ECC has a number of attractive properties. Most unique is the high tensile ductility several hundred times that of concrete while maintaining the compressive strengths similar to concrete or high strength concrete. The metal-like behavior of ECC is achieved without depending on high fiber content, thus breaking the conventional wisdom of the need for high fiber volume fraction to achieve high material performance. The moderate fiber content (2% or less by volume) makes ECC easily adaptable to construction project execution in the field or to precast plant structural element production. Indeed, ECC has demonstrated to possess flexibility in processing routes, including on-site self-consolidating casting, and spraying, as well as off-site precasting and extrusion. Maintaining a moderately low fiber content is obviously important also for economic reasons (Li, 2004).

The large tensile ductility of ECC allows it to deform compatibly and creates a synergistic load sharing capability with steel reinforcement in structural members. As a result, steel reinforcements in R/ECC members are better utilized in enhancing structural performance. Simultaneously, the tight crack width of ECC protects the steel reinforcement from typical corrosive processes, resulting in improved structural durability.

In recent years, a number of full-scale applications of ECC have been carried out in various countries. Foremost amongst these is the use of ECC in precast R/ECC coupling beams in the core of two high rises in Japan (Maruta et al, 2005; Kunieda and Rokugo, 2006b). This application exploits the high energy absorption capability of R/ECC to aid in seismic resistance of these tall buildings. Other notable applications include cast in place ECC link slabs on bridge decks (Kim et al, 2004; Lepech and Li, 2005) in the US and Italy, a composite ECC/Steel bridge deck in Japan (Mitamura et al, 2005), sprayed ECC tunnel linings in South Korea (Wonha, 2004), repair of the Mitaka Dam in Japan

(Kojima et al, 2004), an irrigation channel repair in Japan (Kunieda and Rokugo, 2006b), and prototype pipe extrusion in Australia. Several projects in the housing and in the energy industries employing ECC are in various planning stages. Despite the advanced stage of development of ECC and its application readiness, a great deal of research and experimentation remains. Indeed, the transformation of brittle concrete to ductile ECC offers enormous opportunities in structural innovations not possible previously.

While safety and durability are critically important in any successful engineering project, concerns for sustainability have been increasing due to the greater recognition of the impact of the built environment on the natural environment. Green ECC employing industrial byproducts as components are being developed (Li et al, 2004; Lepech and Li, 2007, Yang et al, 2007). Combined with the greater durability of ECC, such advancements provide a pathway for reducing environment burdens due to transportation infrastructure such as bridges and pavements (Keoleian et al, 2005; Lepech, 2006; Li et al, 2008). Sustainable infrastructures are critical to sustainable economic development in developed and developing countries. Materials technological advancements must contribute to this worldwide effort.

Acknowledgements

The author would like to acknowledge the research support of the National Science Foundation (the Biocomplexity program, the Cyberinfrastructure program and the Civil, Mechanical and Manufacturing Innovation program), and the Michigan Department of Transportation. Many former and current students, post-doctorates, and colleagues at the University of Michigan contributed to this work. Their devotion to advancing infrastructure materials is greatly appreciated. Knowledge on ECC has been greatly expanded by the intense research activities of many academic and industrial groups around the world in the last several years.

Special thanks are extended to Dr. M. Lepech who reviewed a draft of this manuscript and provided helpful suggestions for improvements.

References

- AASHTO LRFD *Bridge Design Specifications*, 3rd 3d., AASHTO, Washington, D.C, 2004.
- Allen, H.G. 1971. Stiffness and strength of two glass-fiber reinforced cement laminates. *Journal of Composite Materials* 5(2):194-207.
- Aveston, J., Cooper, G.A., and Kelly, A. 1971. Single and multiple fracture. In *The Properties of Fiber Composites, Conf. Proc.*, pp.15-24. IPC Science and Technology Press Ltd.
- Bache, H. 1981. Densified cement/ultra-fine particle-based materials, *CBL Rapport Nr. 40*, Aalborg Portland, ISBN 87-89132-00-9.
- Beeldens, A. and Vandewalle, L. 2001. Durability of high strength concrete for highway pavement restoration. In *CONSEC '01: Third International Conference on Concrete under Severe Conditions*, pp. 1230-1238, Vancouver, BC; Canada.

- Billington, S.L. and Yoon, J.K. 2004. Cyclic response of precast bridge columns with ductile fiber-reinforced concrete. *ASCE J. Bridge Eng.*, 9(4):353-363.
- Boshoff, W.P. and van Zijl, G.P.A.G. 2007. Tensile creep of SHCC. In *Proceedings, Fifth International RILEM Workshop on High Performance Fiber Reinforced Cement Composites (HPFRCC 5)*, Reinhardt and Naaman, eds., pp. 87-96.
- Carpinteri, A., Gamarova, P., Ferro, G. and Plizzari, G., eds. 2007. *Proc., Fracture Mechanics of Concrete and Concrete Structures 6*, pp 1883. Taylor & Francis.
- Chanvillard, G. and Rigaud, S. 2003. Complete characterization of tensile properties of ductal UHPFRC according to the French recommendations. In *Proc. of High Performance Fiber Reinforced Cement Composites (HPFRCC4)*, A.E. Naaman and H.W. Reinhardt, eds, pp. 21-34. RILEM Publications S.A.R.L.
- Curbach, M. and Jesse, F. 1999. *High-Performance Textile-Reinforced Concrete, Structural Engineering International* 9(4, 1):289-291(3).
- Fischer, G. and Li, V.C. 2002a. Effect of matrix ductility on deformation behavior of steel reinforced ECC flexural members under reversed cyclic loading conditions. *ACI Structural J.* 99 (6):781-790.
- Fischer, G. and Li, V.C. 2002b. Influence of matrix ductility on the tension-stiffening behavior of steel reinforced engineered cementitious composites (ECC). *ACI Structural J.* 99(1):104-111.
- Fischer, G., and Li, V.C. 2003a. Deformation Behavior of Fiber-Reinforced Polymer Reinforced Engineered Cementitious Composite (ECC) Flexural Members under Reversed Cyclic Loading Conditions. *ACI Structural J.*, 100(1):25-35.
- Fischer, G., and Li, V.C. 2003b. Intrinsic Response Control of Moment Resisting Frames Utilizing Advanced Composite Materials and Structural Elements. *ACI Structural J.*, 100(2):166-176.
- Fischer, G. and Li, V.C., eds. 2006. *Proceedings, International RILEM Workshop on High Performance Fiber Reinforced Cementitious Composites in Structural Application.* pp. 580. RILEM Publications SARL.
- Fischer, G., Wang, S. and Li, V.C. 2003. Design of engineered cementitious composites for processing and workability requirements. *Seventh International Symposium on Brittle Matrix Composites*, pp. 29-36. Warsaw, Poland.
- Fukuyama, H., Iso, M., Ogaw, A. and Suwada, H. 2007. Mitigation of damage due to crack of RC elements utilizing high performance fiber reinforced cementitious composites. In *Proc. of High Performance Fiber Reinforced Cement Composites 5 (HPFRCC 5)*, Reinhardt and Naaman, eds., pp. 427-435. RILEM Publication S.A.R.L.
- Fukuyama, H., Matsuzaki, Y., Nakano, K. and Sato, Y. 1999. Structural performance of beam elements with PVA-ECC. In *Proc. of High Performance Fiber Reinforced Cement Composites 3 (HPFRCC 3)*, Reinhardt and A. Naaman, eds., pp. 531-542. Chapman & Hull.
- Fukuyama, H., Matzuzaki, Y., Sato, Y., Iso, M. and Suwada, H. 2000. Structural performance of engineered cementitious composite elements. *Composite and Hybrid Structures, 6th ASCCS Int'l Conf. on Steel-Concrete Composite Structures*, pp. 969-976.
- Fukuyama, H., Suwada, H. and Mukai, T. 2006. Test on High-Performance Wall Elements with HPFRCC, In *Proc., Int'l RILEM Workshop HPFRCC in Structural*

- Applications*, Eds. Fischer, G., and V.C. Li, published by RILEM SARL, pp. 365-374.
- Horikoshi, T., Ogawa, A., Saito, T., and Hoshiro, H. 2006. Properties of Polyvinylalcohol fiber as reinforcing materials for cementitious composites, in *Proc., Int'l RILEM Workshop on High Performance Fiber Reinforced Cementitious Composites in Structural Application*, RILEM Publications SARL, pp. 145-153.
- JSCE (Japan Society of Civil Engineers), 2007. *Recommendations for Design and Construction of High Performance Fiber Reinforced Cement Composite with Multiple Fine Cracks (Draft)*, (in Japanese).
- Kabele, P., 2001. Assessment of Structural Performance of Engineered Cementitious Composites by Computer Simulation. *CTU Reports 4/2001*, (4):1-100. ISBN 80-01-02500-4. Prague: CTU.
- Kabele, P., and Kanakubo, T., 2007. Experimental and Numerical Investigation of Shear Behavior of PVA-ECC in Structural Elements. In *Proceedings, Fifth International RILEM Workshop on High Performance Fiber Reinforced Cement Composites (HPFRCC 5)*, Reinhardt and Naaman, eds., pp. 137-146.
- Kabele, P., Novak, L., Nemecek, J. and Pekar, J. 2007. Multiscale experimental investigation of deterioration of fiber-cementitious composites in aggressive environment. In *Proc. MHM 2007: Modelling of Heterogeneous Materials, with Applications in Construction and Biomedical Engineering*, M. Jirasek, Z. Bittnar and H. Mang, eds, pp. 270-271.
- Kamal, A., Kunieda, M., Ueda, N., and Nakamura, H. 2007. Assessment of Crack Elongation Performance in RC Beam Repaired by UHP-SHCC. In print, in Proc. ASCE Int'l Summer Symposium.
- Kanakubo, T. 2006. Tensile characteristics: evaluation method for DFRCC," *Journal of Advanced Concrete Technology* 4 (1):3-17.
- Kanda, T. and Li, V.C. 1999. A new micromechanics design theory for pseudo strain hardening cementitious composite. *ASCE J. of Engineering Mechanics* 125(4):373-381.
- Kanda, T., Kanakubo, T., Nagai, S., and Maruta, M. 2006a. Technical consideration in producing ECC pre-cast structural elements. In *Proc., International RILEM Workshop on High Performance Fiber Reinforced Cementitious Composites in Structural Applications*, G. Fischer and V.C. Li, eds., pp. 229-242. RILEM Publications SARL.
- Kanda, T., Tomoe, S., Nagai, S., Maruta, M., Kanakubo, T., and Shimizu, K. 2006b. Full Scale Processing Investigation for ECC Pre-cast Structural Element, *J. of Asian Architecture and Building Engineering* 5 (2): 333-340.
- Kanda, T. and Li V.C. 2001. Practical design criteria for saturated pseudo strain hardening behavior in ECC. *J. Advanced Concrete Technology* 4(1):59-72.
- Kanda, T., Saito, T., Sakat, N. and Hiraishi, H. 2001. Basic properties of sprayed repair material based on a highly ductile FRC with PVA fiber. In *Proc. Of the annual meeting of JCI* 25(1):475-480.
- Kanda, T., Watanabe, S. and Li, V.C. 1998. Application of pseudo strain hardening cementitious composites to shear resistant structural elements. In *Fracture Mechanics of Concrete Structures Proceedings FRAMCOS-3*, pp. 1477-1490. AEDIFICATIO Publishers, D-79104 Freiburg, Germany.

- Keoleian, G.A., Kendall, A., Dettling, J.E., Smith, V.M., Chandler, R., Lepech, M.D. and Li, V.C. 2005. Life cycle modeling of concrete bridge design: comparison of engineered cementitious composite link slabs and conventional steel expansion joints. *ASCE J. Infrastructure Systems* 11(1):51-60.
- Kesner, K.E. and Billington, S.L. 2005. Investigation of infill panels made from engineered cementitious composites for seismic strengthening and retrofit. *ASCE J. Structural Engineering* 131(11): 712-1720.
- Kim, Y.Y., Kong, H.J. and Li, V.C. 2003. Design of engineered cementitious composite (ECC) suitable for wet-mix shotcreting. *ACI Materials J*, 100 (6):511-518.
- Kim, Y.Y., Fischer, G. and Li, V.C. 2004. Performance of bridge deck link slabs designed with ductile ECC. *ACI Structural J*. 101(6):792-801.
- Kojima, S., Sakat, N., Kanda, T. and Hiraishi, T. 2004. Application of direct sprayed ECC for retrofitting dam structure surface – application for Mitaka-Dam. *Concrete Journal* 42(5):35-39. (In Japanese).
- Kong, H.J., Bike, S. and Li, V.C. 2003. Development of a self-compacting engineered cementitious composite employing electrosteric dispersion/stabilization. *J. Cement and Concrete Composites* 25(3):301-309.
- Krenchel, H. and Stang, H. 1989. Stable microcracking in cementitious materials. In *Brittle Matrix Composites 2*. A.M. Brandt and J.H. Marshall, eds., pp. 20-33. Elsevier Applied Science.
- Kunieda, M. and Rokugo, K. 2006a. Measurement of crack opening behavior within ECC under bending moment. In *Proc., Int'l RILEM Workshop HPFRCC in Structural Applications*, Eds. Fischer, G., and V.C. Li, published by RILEM SARL, pp. 313-322.
- Kunieda, M. and Rokugo, K. 2006b. Recent progress on HPFRCC in Japan – Required performance and applications. *J. Advanced Concrete Technology* 4(1):19-33, Japan Concrete Institute.
- Lankard, D.R. 1986. Preparation, properties and applications of cement based composites containing 5-20 percent steel fiber reinforcement. In *Steel Fiber Concrete*, S.P. Shah, S.P. and A. Skarendahl, eds. Elsevier Publishers.
- Lepech, M.D. 2006. A paradigm for integrated structures and materials design for sustainable transportation infrastructure. PhD Thesis, University of Michigan, Ann Arbor, MI.
- Lepech M.D. and Li, V.C. 2005. Water permeability of cracked cementitious composites. *Proceedings of Eleventh International Conference on Fracture*, Turin, Italy. March 20-25.
- Lepech, M.D. and Li, V.C. 2005. Design and field demonstration of ECC link slabs for jointless bridge decks. *ConMat'05*, Vancouver, Canada, CD-documents/1-05/SS-GF-05_FP.pdf.
- Lepech, M.D. and Li, V.C. 2007. Large scale processing of engineered cementitious composites. Accepted, *ACI Materials J.*, July 2007.
- Lepech, M.D., Li, V.C., Robertson, R.E. and Keoleian, G.A. 2007. Design of ductile engineered cementitious composites for improved sustainability. Submitted to the *ACI Materials J.*

- Leung, C.K.Y., Cheung, A.K.F., and Zhang, X. 2006. Partial use of pseudo-ductile cementitious composites in concrete components to resist concentrated stress, *Key Engineering Materials*, 312, 319-324.
- Li, M., Şahmaran, M., and Li, V.C. 2007. Effect of cracking and healing on durability of engineered cementitious composites under marine environment. In *Proc., High Performance Fiber Reinforced Cement Composites (HPFRCC5)*, H.W. Reinhardt and A.E. Naaman, eds., pp. 313-322. Mainz, Germany.
- Li, V.C. 1993. From Micromechanics to Structural Engineering – the design of cementitious composites for Civil Engineering applications. *JSCE J. of Struc. Mechanics and Earthquake Engineering* 10(2):37-48.
- Li, V.C. 2000. When a crack is not a crack. In *Proc., BMC6*, A. Brandt, I. Marshall, and V.C. Li, eds., pp. 173-185.
- Li, V.C. 2004. Strategies for high performance fiber reinforced cementitious composites development. In *Fiber Reinforced Concrete: From Theory to Practice*, Proc. N. American/European Workshop on Advances in Fiber Reinforced Concrete, S. Ahmad, M. di Prisco, C. Meyer, G.A. Plizzari, and S. Shah, eds., pp. 93-98. Bergamo, Italy.
- Li, V.C. 2007. Integrated structures and materials design. *RILEM J. of Materials and Structures* 40(4):387-396.
- Li, V.C., Fischer, G., Kim, Y.Y., Lepech, M., Qian, S., Weimann, M., Wang, S. 2003. Durable link slabs for jointless bridge decks based on strain-hardening cementitious composites. Report for Michigan Department of Transportation RC-1438.
- Li, V.C., Horikoshi, T., Ogawa, A., Torigoe, S. and Saito, T. 2004. Micromechanics-based durability study of polyvinyl alcohol-engineered cementitious composite (PVA-ECC). *ACI Materials J.* 101(3)242-248.
- Li, V.C. and Lepech, M. 2004. Crack resistant concrete material for transportation construction. In *TRB 83rd Annual Meeting, Washington, D.C., Compendium of Papers CD ROM*, Paper 04-4680.
- Li, V.C., Lepech, M., Wang, S., Weimann, M. and Keoleian, G. 2004. Development of green ECC for sustainable infrastructure systems. In *Proc., Int'l Workshop on Sustainable Development and Concrete Technology*, Beijing, China, K. Wang, ed., pp. 181-192. Iowa State Univ.
- Li, V.C. and Leung, C.K.Y. 1992. Steady state and multiple cracking of short random fiber composites. *ASCE J. of Engineering Mechanics*, 118 (11):2246-2264.
- Li, V.C., Qian, S., Zhang, H., and Keoleian, G.A. 2008. Sustainable infrastructure with durable fibre concrete material. *Congress 2008 - Concrete: Construction's Sustainable Option*. Dundee Scotland.
- Li, V.C., and Stang, H. 2004. Elevating FRC Material Ductility to Infrastructure Durability,” in *Fiber-Reinforced Concretes*, Proc, BEFIB 2004, Ed. M.di Prisco, R. Felicetti and G.A. Plizzari, pp. 171-186.
- Li, V.C. and Yang, E.H. 2007. Self-healing in concrete materials. In *Self Healing Materials: An Alternative Approach to 20 Centuries of Materials Science*, S. van der Zwaag, ed., pp161–193. Springer.
- Li, V.C. and Wang, S. 2002. Failure mode and structural ductility of GFRP reinforced engineered cementitious composite beams. *ACI Materials J.* 99(1):11-21.

- Li, V.C. and Wang, S. 2006. Microstructure Variability and Macroscopic Composite Properties of High Performance Fiber Reinforced Cementitious Composites. *J. Probabilistic Engineering Mechanics* 21(3):201-206.
- Li, V.C., Wu, C., Wang, S., Ogawa, A. and Saito, T. 2002. Interface tailoring for strain-hardening PVA-ECC. *ACI Materials J.* 99(5):463-472.
- Li, V.C., Wu, H.C., and Chan, Y.W. 1996. Effect of Plasma Treatment of Polyethylene Fibers on Interface and Cementitious Composite Properties. *J. of Amer. Ceramics Soc.*, 79 (3):700-704.
- Lim, Y.M. and Li, V.C. 1997. Durable repair of aged infrastructures using trapping mechanism of engineered cementitious composites. *J. Cement and Concrete Composites* 19(4):373-385.
- Maalej, M. and Li, V.C. 1994. Flexural/Tensile Strength Ratio in Engineered Cementitious Composites. *ASCE J. of Materials in Civil Engineering*, 6(4):513-528.
- Maalej, M., and Li, V.C. 1995. Introduction of Strain Hardening Engineered Cementitious Composites in the Design of Reinforced Concrete Flexural Members for Improved Durability. *ACI Structural J.*, 92(2):167-176.
- Maruta, M., Kanda T., Nagai S. and Yamamoto, Y. 2005. New high-rise RC structure using pre-cast ECC coupling beam. *Concrete Journal* 43(11):18-26.
- Martinola, G., Baeuml, M.F., Wittmann, F.H. 2004. Modified ECC by means of internal impregnation. *J. Advanced Concrete Technology* 2(2): 207-212.
- Mechtcherine, V., and Lieboldt, M. 2007. Effect of cracking on air-permeability and water absorption of strain hardening cement-based composites. In *Proceedings, Fifth International RILEM Workshop on High Performance Fiber Reinforced Cement Composites (HPFRCC 5)*, Reinhardt and Naaman, eds., pp. 305-312.
- Mechtcherine, V., and Schulze, J. 2006. Testing the behavior of strain hardening cementitious composites in tension. In *Proceedings, International RILEM Workshop on High Performance Fiber Reinforced Cementitious Composites in Structural Applications*, G. Fischer and V.C. Li, eds., pp 37-46. RILEM Publications SARL.
- Mehta, P.K. and Monteiro, P.J.M. 2006. *Concrete: Structure, Properties, and Materials*, 3rd ed. The McGraw Hill Companies, Inc., New York.
- Mihashi, H. and De Leite, J.P.B. 2004. State-of-the-art report on control of cracking in early age concrete. *Advanced Concrete Technology* 2(2):141-154.
- Mitamura, H., Sakata, N., Shakushiro, K., Suda, K. and Hiraishi, T. 2005. Application of overlay reinforcement method on steel deck utilizing engineering cementitious composites – Mihara Bridge. *Bridge and Foundation Engineering* 39(8):88-91.
- Miyazato S. and Hiraishi, Y. 2005. Transport properties and steel corrosion in ductile fiber reinforced cement composites. *Proc. ICF 11*, Torino, Italy.
- Mobasher, B., Peled, A. and Pahilajani, J. 2006. Distributed cracking and stiffness degradation in fabric-cement composites. *Materials and Structures*, 39:317-331.
- Mora, J., Aguado, A., Gettu, R. 2003. The influence of shrinkage reducing admixtures on plastic shrinkage. *Materiales de Construcción* 53(271-272):71-80.
- Naaman, A.E. 1992. SIFCON: Tailored properties for structural performance. In *High Performance Fiber Reinforced Cement Composites*, H.W. Reinhardt and A.E. Naaman, eds., pp. 18-38. Published by E & FN Spon, London.
- Naaman, A.E. and Reinhardt, H.W. 2003. Setting the stage: toward performance-based classification of FRC composites. In *High Performance Fiber Reinforced Cement*

- Composites (HPFRCC-4)*, Proc. Of the 4th Int'l RILEM Workshop, A.E. Naaman and H.W. Reinhardt, eds. Published by RILEM S.A.R.L.
- Nemecek, J., Kabele, P., Kopecky, L., and Bittnar, Z. 2006. Leached Engineered Cementitious Composites, Proc., Int'l RILEM Workshop on High Performance Fiber Reinforced Cementitious Composites in Structural Application. Eds. Fischer, G., and V.C. Li, published by RILEM SARL. pp.205-212.
- Neville, A.M. 1995. *Properties of Concrete*. 4th ed., Longman Group Limited.
- Oh, B.H., Cha, S.W., Jang, B.S., Jang, S.Y. 2002. Development of high-performance concrete having high resistance to chloride penetration. *Elsevier Science SA, Nuclear Engineering and Design (Switzerland)* 212(1-3):221-231.
- Oh, B.H., and Shin, K.J. 2006. Cracking, ductility and durability characteristics of HPFRCC with various mixture proportions and fibers, in Proc., Int'l RILEM Workshop on High Performance Fiber Reinforced Cementitious Composites in Structural Application. Eds. Fischer, G., and V.C. Li, Eds. Fischer, G., and V.C. Li, published by RILEM SARL, pp. 213-222.
- Parra-Montesinos, G. and Wight, J.K. 2000. Seismic response of exterior RC column-to-steel beam connections. *ASCE Journal of Structural Engineering* 126(10):1113-1121.
- Proctor, B.A., Oakley, D.R., and Litherland, K.L., 1982. Developments in the assessment and performance of GRC over 10 Years. *Composites*, 173.
- Qian, S. 2007. Influence of Concrete Material Ductility on the Behavior of High Stress Concentration Zones, PhD Thesis, Univ. of Michigan, Ann Arbor, MI.
- Qian, S. and Li, V.C. 2006. Influence of Concrete Material Ductility on the Shear Response of Stud Connection. *ACI Materials J.*, 103(1):60-66.
- Qian, S. and Li, V.C. 2007. Simplified inverse method for determining the tensile strain capacity of strain hardening cementitious composites. *J. Advanced Concrete Technology* 5(2):235-246.
- Reinhardt, H. and A.E. Naaman, eds. 2007. *Proceedings, High Performance Fiber Reinforced Cement Composites (HPFRCC5)*, pp. 518. Published by RILEM.
- Reinhardt, H.W., Krüger, M. and Große, C.U. 2003. Concrete prestressed with textile fabric. *Journal of Advanced Concrete Technology* 1(3):231-239.
- Rokugo, K., Kanda, T., Yokota, H. and Sakata, N. 2007. Outline of JSCE recommendation for design and construction of multiple fine cracking type fiber reinforced cementitious composite (HPFRCC). In *Proceedings, Fifth International RILEM Workshop on High Performance Fiber Reinforced Cement Composites (HPFRCC 5)*, Reinhardt and Naaman, eds., pp. 203-212.
- Rokugo, K., Kunieda, M., Lim, S.C. 2005. Patching repair with ECC on cracked concrete surface. *Proc. CONMAT 5*.
- Romualdi, N.P. and Batson, G.B. 1963. Mechanics of crack arrest in concrete. *Proc. ASCE Eng. Mech. J.* 89(EM3):147-168.
- Romualdi, J.P. and Mandel, J.A. 1964. Tensile strength of concrete affected by uniformly distributed closely spaced short lengths of wire reinforcement. *Proc. ACI J.* 61(6):657-671.
- Şahmaran, M., Li, M. and Li, V.C. 2007. Transport properties of engineered cementitious composites under chloride exposure. In print, *ACI Materials J.*

- Şahmaran , M. and Li, V.C. 2007a. De-icing salt scaling resistance of mechanically loaded engineered cementitious composites. *J. Cement and Concrete Research* 37:1035-1046.
- Şahmaran , M. and Li, V.C. 2007b. Durability of mechanically loaded engineered cementitious composites under high alkaline environment. Submitted, *J. Cement and Concrete Composites*, March, 2007.
- Şahmaran , M. and Li, V.C. 2007c. Influence of microcracking on water absorption and sorptivity of ECC. Submitted, *RILEM J. of Materials and Structures*, Aug., 2007.
- Şahmaran , M., Li, V.C. and Andrade, C. 2006. Corrosion resistance performance of steel-reinforced engineered cementitious composites beams. Submitted, *ACI Materials J.*, Dec., 2006.
- Shimizu, K., Kanakubo, T., Kanda, T., and Nagai, S. 2006. in *Proc., Int'l RILEM Workshop HPFRCC in Structural Applications*, Eds. Fischer, G., and V.C. Li, published by RILEM SARL, pp. 443-451.
- Stang, H. and Li, V.C. 1999. Extrusion of ECC-Material. In *Proc., High Performance Fiber Reinforced Cement Composites 3 (HPFRCC 3)*, H. Reinhardt & A. Naaman, eds., pp. 203-212. Chapman & Hull.
- Stang, H., and Li, V.C. 2004. Classification of Fiber Reinforced Cementitious Materials for Structural Applications,” in *Fiber-Reinforced Concretes*, Proc, BEFIB 2004, Ed. M.di Prisco, R. Felicetti and G.A. Plizzari, pp. 197-218.
- Suthiwarapirak, P., Matsumoto, T., and Kanda, T., 2002. Flexural fatigue failure characteristics of an engineered cementitious composite and polymer cement mortars. *JSCE J. Materials, Conc. Struc. Pavements*, 718(57):121-134.
- Szerszen, M.M., Szwed, A. and Li, V.C. 2006. Flexural response of reinforced beam with high ductility concrete material. In Proc. Int. Symp. “*Brittle Matrix Composites 8*.” A.M. Brandt, V.C. Li and I.H. Marshall, eds., pp. 263-274. Woodhaed Publ., Warsaw.
- Vandewalle, L., et al, 2003. RILEM TC 162-TDF: Test and design methods for steel fibre reinforced concrete' - sigma-epsilon-design method - Final Recommendation. *Materials and Structures* 36(262):560-567.
- Walter, R., Li, V.C. and Stang, H. 2004. Comparison of FRC and ECC in a composite bridge deck. In *Proc., 5th PhD Symposium in Civil Engineering*, pp. 477-484, 2004. Delft, The Netherlands.
- Wang, S. 2005. Micromechanics based matrix design for engineered cementitious composites, PhD Thesis, University of Michigan.
- Wang, S. and Li, V.C. 2003. Materials design of lightweight PVA-ECC. In *Proc., HPFRCC*, A.E. Naaman and H.W. Reinhardt, eds., pp.379-390. Ann Arbor, MI.
- Wang, S. and Li, V.C. 2006a. High early strength engineered cementitious composites. *ACI Materials J.* 103(2):97-105.
- Wang, S. and Li, V.C., 2006b. Polyvinyl Alcohol Fiber Reinforced Engineered Cementitious Composites: Material Design and Performances, in *Proc., Int'l RILEM Workshop HPFRCC in Structural Applications*, Eds. Fischer, G., and V.C. Li, published by RILEM SARL, pp. 65-73.
- Weiss, W.J. and Shah, S.P. 2002. Restrained shrinkage cracking: the role of shrinkage reducing admixtures and specimen geometry. *Materials and Structures* 35(246):85-91.

- Wittmann, F.H. 2002. Crack formation and fracture energy of normal and high strength concrete. *Sadhana* 27(4):413-423.
- Wonha Engineering & Construction Co., Ltd., Korea, Private Communications, 2005.
- Yang, Y., Lepech, M. and Li, V.C. 2005. Self-healing of engineered cementitious composites under cyclic wetting and drying. In *Proc. Int. Workshop on Durability of Reinforced Concrete under Combined Mechanical and Climatic Loads (CMCL)*, pp. 231-242. Qingdao, China.
- Yang, E.H. and Li, V.C. 2007. Strain-hardening fiber cement optimization and component tailoring by means of a micromechanical model. Accepted, *J. Construction and Building Materials*.
- Yang, E.H., Yang, Y. and Li, V.C. 2007. Use of high volumes of fly ash to improve ECC mechanical properties and material greenness. In print, *ACI Materials J.*.

Table of Figures

FIGURE 24.1: Uniaxial tensile stress-deformation relation of concrete, FRC, and HPFRCC. For FRC, deformation after a crack is formed is associated with crack opening δ . Tensile load capacity drops as a single crack enlarges during tension-softening. For HPFRCC, deformation during the elastic and strain-hardening stages is properly described as straining. Tensile load capacity continues to rise during multiple microcracking and continued increase in strain. The strain capacity of HPFRCC is defined as the strain value at which peak tensile load is reached.

FIGURE 24.2: Two classes of HPFRCCs. (a) Tensile stress-elongation relationship for high strength Ductal[®] (after Chanvillard and Rigaud, 2003) based on prism specimen with 70x70x160 mm with 150 mm gage length. (b) & (c) Tensile Stress-Strain relationship for ductile ECC (adapted from Fischer et al, 2003 and Li and Wang, 2002), based on coupon specimen 76x13x305 mm with 180 mm gage length.

FIGURE 24.3: A tensile stress-strain curve of an ECC, showing also the crack width development as a function of imposed tensile strain.

FIGURE 24.4: Illustration of the energy criterion for multiple cracking: (a) When Eq. (24.1b) is not satisfied, the common Griffith-type crack propagation results. Cracking opening at the middle δ_m will exceed δ_0 causing spring failure and subsequent tension-softening, and (b) When Eq. (24.1b) is satisfied, the steady state flat crack propagation mode prevails, with δ_{ss} staying below δ_0 .

FIGURE 24.5: (a) Compressive strength development of ECC (M45), and (b) ECC specimen after compressive strength test (Wang and Li, 2006b).

FIGURE 24.6: (a) Flexural load-deflection curve of an ECC, and (b) ECC flexural specimen showing large deflection, and (c) Fine multiple cracking on the tensile side of beam of 304 mm (length) x 76.2 mm (width) x 25.4 mm (depth) (after Wang and Li, 2006b).

FIGURE 24.7: Creamy texture appearance of fresh ECC in mixing drum of a ready-mix truck (Lepech and Li, 2007).

FIGURE 24.8: (a) Slump cone test of ECC flowability, and (b) Marsh cone flow rate test.

FIGURE 24.9: Various processing methods of ECC: (a) Self-consolidating casting, (b) extrusion, and (c) spraying, (d) precast mixing (Photo: courtesy of S. Staniski) and precasted element.

FIGURE 24.10: Test set up for full reversed loading of flexural elements (Fischer and Li, 2002a).

FIGURE 24.11: Specimen configurations of flexural elements (a) R/C and (b) R/ECC with no stirrups in shear zone (Fischer and Li, 2002a).

FIGURE 24.12: Hysteretic behavior of flexural members under fully reversed cyclic loading for (a) R/C with stirrups, and (b) R/ECC without stirrups (Fischer and Li, 2002a).

FIGURE 24.13: Damage behavior of (a) R/C and (b) R/ECC without stirrups, shown at 10% drift (Fischer and Li, 2002a).

FIGURE 24.14: Flexural fatigue testing of ECC link-slab element (Kim et al, 2004).

FIGURE 24.15: Stiffness and crack width change as a function of load cycles. LS-1 is the control R/C specimen. LS-2 and LS-3 are both R/ECC specimens with different reinforcement details to represent new and retrofit construction conditions (Kim et al, 2004).

FIGURE 24.16: Composite steel/ECC beam test set-up (Walter et al, 2005).

FIGURE 24.17: Load and debonding as a function of composite beam deflection (Walter et al, 2005). Significant increase in load capacity and delay in debonding was achieved in the steel/ECC beam versus the steel/FRC and steel/FRD beams.

FIGURE 24.18: Fully reversed Ohno shear test set-up (Fukuyama et al, 2000).

FIGURE 24.19: Hysteretic loops for Ohno shear beams under fully reversed cyclic loading for (a) R/C, and (b) R/ECC (Fukuyama et al, 2000).

FIGURE 24.20: Damage pattern in Ohno shear beams (a) R/C, and (b) R/ECC (Fukuyama et al, 2000).

FIGURE 24.21: Hysteretic behavior of columns under fully reversed cyclic loading for (a) R/C, and (b) R/ECC (Fukuyama et al, 2000).

FIGURE 24.22: Test set-up for beam-column connection (Parra-Montesinos and Wight, 2000).

FIGURE 24.23: Hysteretic loops of fully reversed cyclic test on beam-column connections for (a) R/C with stirrups and (b) R/ECC without stirrups (Parra-Montesinos and Wight, 2000).

FIGURE 24.24: The damage behavior of the shear panel of a hybrid connection after cyclic loading (after Parra-Montesinos and Wight 2000). The green squares is enlarged in the inserts for easier viewing of the cracks in (a) R/C, and (b) R/ECC.

FIGURE 24.25: Wall panel test setup (Kesner and Billington, 2005).

FIGURE 24.26: Hysteretic loops of shear wall (after Kesner and Billington, 2005).

FIGURE 24.27: (a) Stress flow before and after matrix cracking, and (b) Left: Brittle fracture of concrete in normal R/C causes unloading of concrete near crack, and a jump in tensile straining the steel locally, resulting in high interfacial shear and bond breakage. Right: In contrast, compatible deformation occurs between ECC and steel reinforcement with no shear lag, thus maintaining integrity of the interfacial bond. (Fischer and Li, 2002b).

FIGURE 24.28: Tensile strain capacity of ECC as a function of age after casting (Li and Lepech, 2004).

FIGURE 24.29: Relative dynamic modulus of normal concrete and three versions of ECC, all without air-entrainment (Li et al, 2003).

FIGURE 24.30: Tensile stress strain curves of ECC (a) virgin coupon specimens and (b) pre-cracked (to 0.5%) specimens and (c) precracked (to 1.5%) specimens, before and after subjected to 3% NaCl solution exposure (Li et al, 2007).

FIGURE 24.31: Effect of freeze-thaw cycles in the presence of de-icing salts for (a) beams preloaded to different bending deformation (BD) levels, showing mass of scaled-off particles, and (b) Coupon specimens preloaded to different levels, showing uniaxial tensile stress-strain curves after 50 cycles of exposure (Şahmaran and Li, 2007a).

FIGURE 24.32: Length Change of ECC Mix (a) with Class F fly ash, and (b) with Class C fly ash subjected to alkali-silicate reaction tests (Şahmaran and Li, 2007b).

FIGURE 24.33: Permeability of precracked ECC and reinforced mortar measured as a function of crack width (after Lepech and Li, 2005).

FIGURE 24.34: Diffusion coefficient versus pre-loading deformation level for ECC and mortar (Şahmaran et al, 2007).

FIGURE 24.35: Capillary transport properties measured for preloaded ECC beams, showing the effects of water repellent on (a) Sorptivity index and (b) Volume of permeable pores, as a function of the number of cracks (Şahmaran and Li, 2007c).

FIGURE 24.36: Measured corrosion rate along the steel rebar for preloaded (a) R/C, and (b) R/ECC (after Miyazato and Hiraishi, 2005).

FIGURE 24.37: ECC and mortar specimens after accelerated corrosion test: (a) ECC prismatic specimen after 300 hours accelerated corrosion, (b) Mortar prismatic specimen after 75 hours accelerated corrosion, (c) ECC cylindrical specimen after 350 hours accelerated corrosion, (d) Mortar cylindrical specimen after 95 hours accelerated corrosion (Şahmaran et al, 2006).

FIGURE 24.38: Types of failure of reinforced mortar and ECC beams under four point bending test for (a) ECC before accelerated corrosion, (b) ECC after 150 hours accelerated corrosion, (c) Mortar before accelerated corrosion, and (d) Mortar after 50 hours accelerated corrosion (after Şahmaran et al, 2006).

FIGURE 24.39: Mass loss versus time for ECC and mortar corrosion specimens (Şahmaran et al, 2006).

FIGURE 24.40: Cracking behavior of patched earth retaining wall (a) Before repair and showing ASR damage, and (b) after repair at 12 months, and (c) after repair at 24 months. Blocks 1-8 used ECC, block 9 use a normal repair mortar, and block 10 was left unrepaired (after Rokugo et al, 2005).

FIGURE 24.41: (a) ECC and concrete patches on the Curtis Road, Ann Arbor bridge deck, (b) Maximum crack width development over time for the two materials. The concrete patch was re-repaired at about 1000 days.

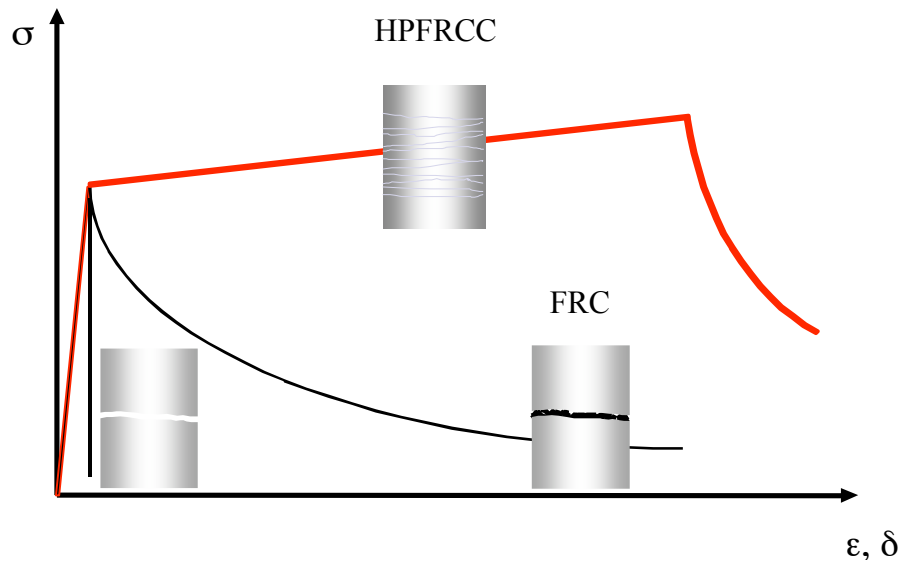
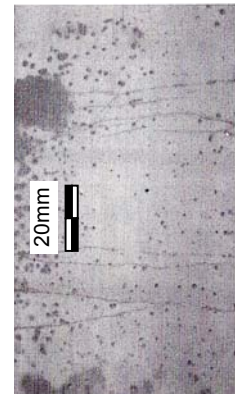
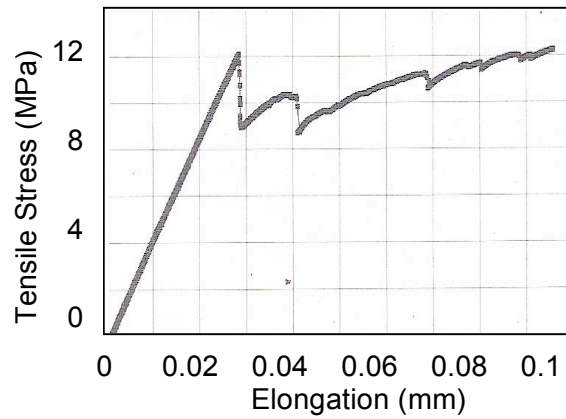
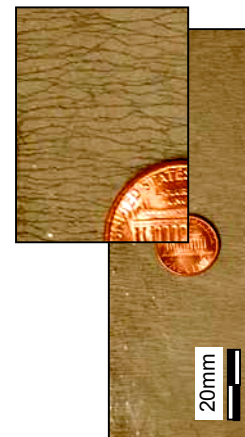
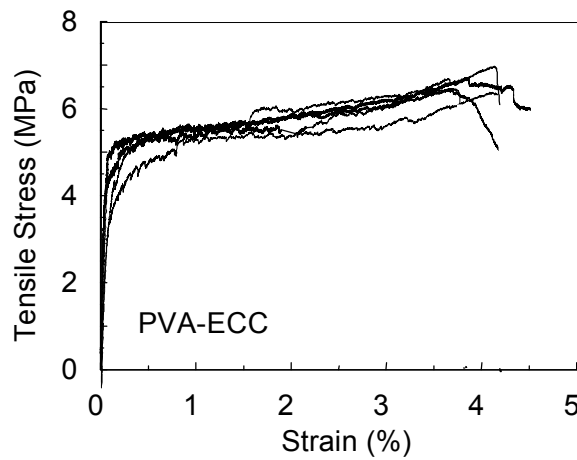


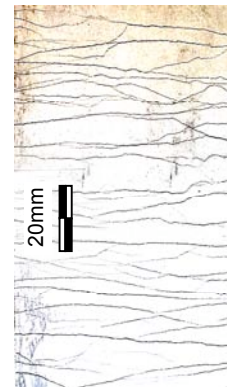
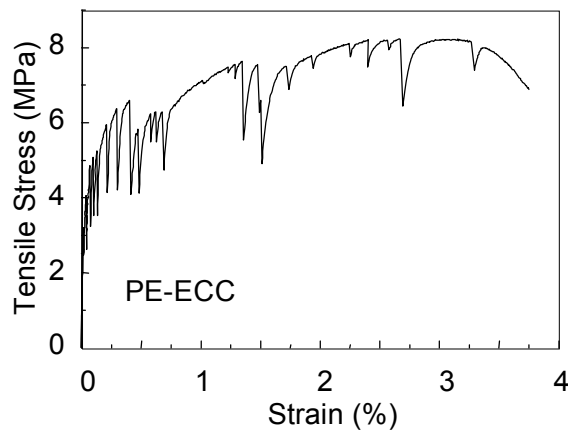
FIGURE 24.1: Uniaxial tensile stress-deformation relation of concrete, FRC, and HPFRCC. For FRC, deformation after a crack is formed is associated with crack opening δ . Tensile load capacity drops as a single crack enlarges during tension-softening. For HPFRCC, deformation during the elastic and strain-hardening stages is properly described as straining. Tensile load capacity continues to rise during multiple microcracking and continued increase in strain. The strain capacity of HPFRCC is defined as the strain value at which peak tensile load is reached.



(a)



(b)



(c)

FIGURE 24.2: Two classes of HPFRCCs. (a) Tensile stress-elongation relationship for high strength Ductal[®] (after Chanvillard and Rigaud, 2003) based on prism specimen with 70x70x160 mm with 150 mm gage length. (b) & (c) Tensile Stress-Strain relationship for ductile ECC (adapted from Fischer et al, 2003 and Li and Wang, 2002), based on coupon specimen 76x13x305 mm with 180 mm gage length.

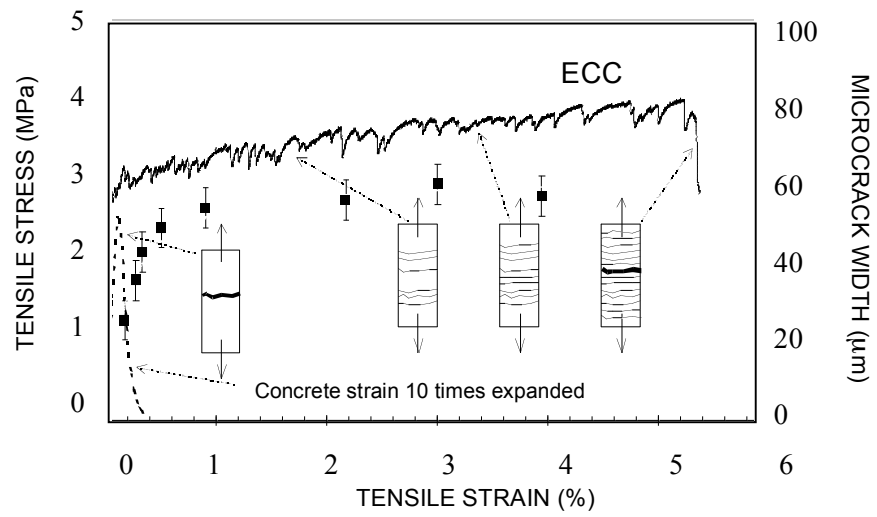


FIGURE 24.3: A tensile stress-strain curve of an ECC, showing also the crack width development as a function of imposed tensile strain.

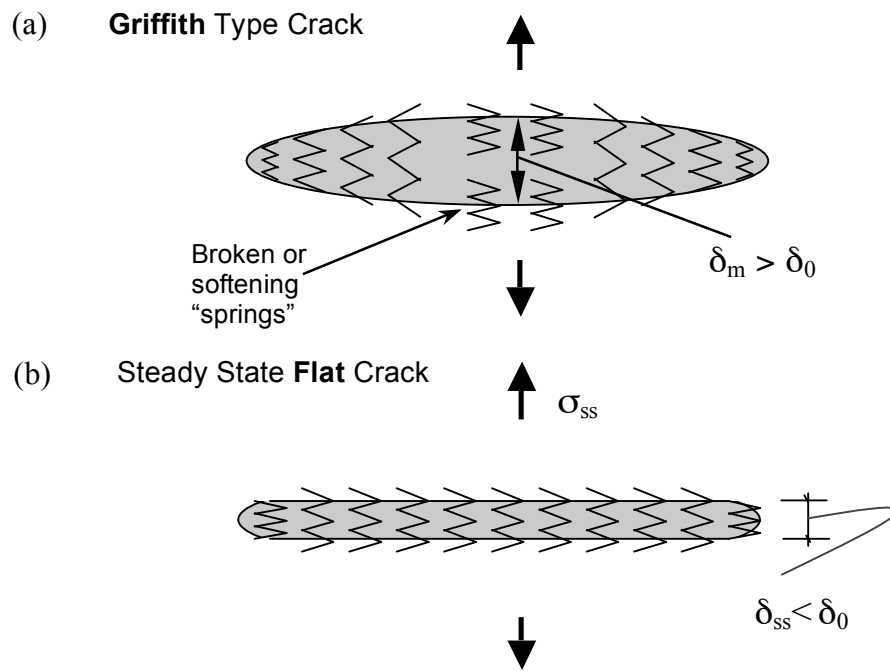
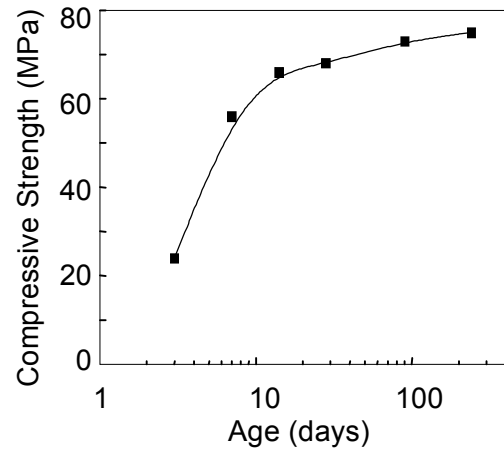


FIGURE 24.4: Illustration of the energy criterion for multiple cracking: (a) When Eq. (24.1b) is not satisfied, the common Griffith-type crack propagation results. Cracking opening at the middle δ_m will exceed δ_0 causing spring failure and subsequent tension-softening, and (b) When Eq. (24.1b) is satisfied, the steady state flat crack propagation mode prevails, with δ_{ss} staying below δ_0 .

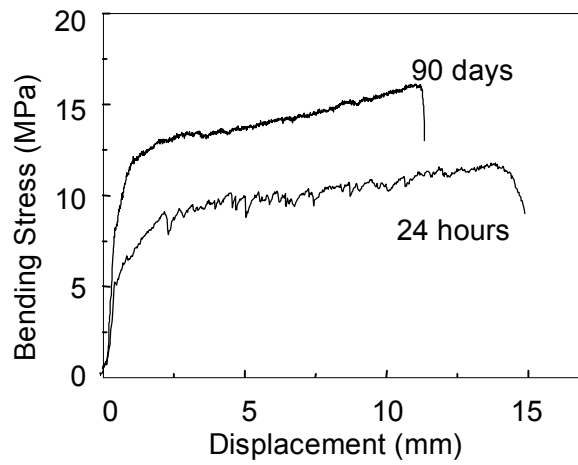


(a)



(b)

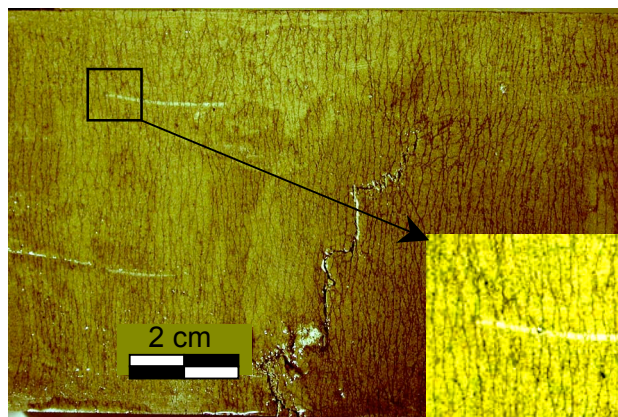
FIGURE 24.5: (a) Compressive strength development of ECC (M45), and (b) ECC specimen after compressive strength test (Wang and Li, 2006b).



(a)



(b)



(c)

FIGURE 24.6: (a) Flexural load-deflection curve of an ECC, and (b) ECC flexural specimen showing large deflection, and (c) Fine multiple cracking on the tensile side of beam of 304 mm (length) x 76.2 mm (width) x 25.4 mm (depth) (after Wang and Li, 2006b).



FIGURE 24.7: Creamy texture appearance of fresh ECC in mixing drum of a ready-mix truck (Lepech and Li, 2007).



(a)



(b)

FIGURE 24.8: (a) Slump cone test of ECC flowability, and (b) Marsh cone flow rate test.



(a)



(b)



(c)

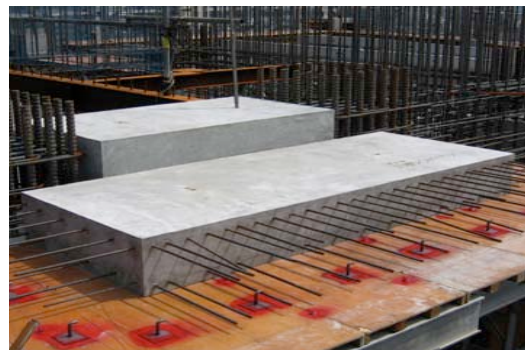


FIGURE 24.9: Various processing methods of ECC: (a) Self-consolidating casting, (b) extrusion, and (c) spraying, (d) precast mixing (Photo: courtesy of S. Staniski) and precasted element.

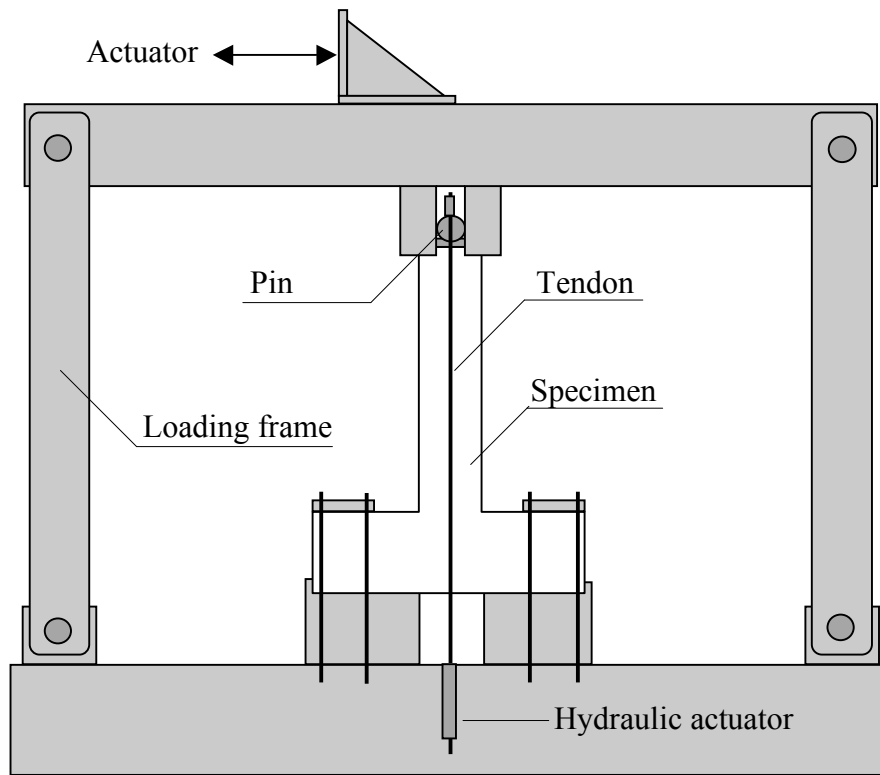


FIGURE 24.10: Test set up for full reversed loading of flexural elements (Fischer and Li, 2002a).

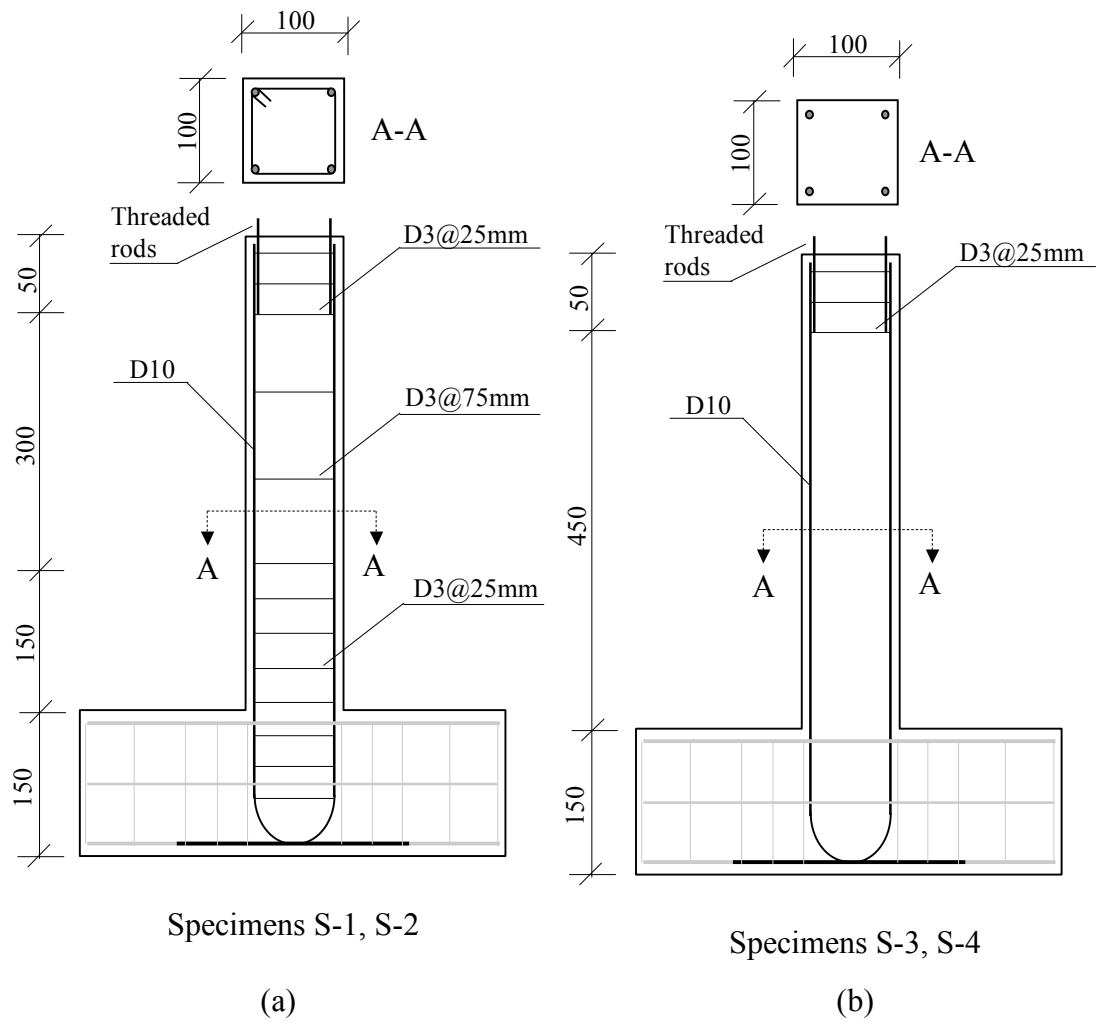


FIGURE 24.11: Specimen configurations of flexural elements (a) R/C and (b) R/ECC with no stirrups in shear zone (Fischer and Li, 2002a).

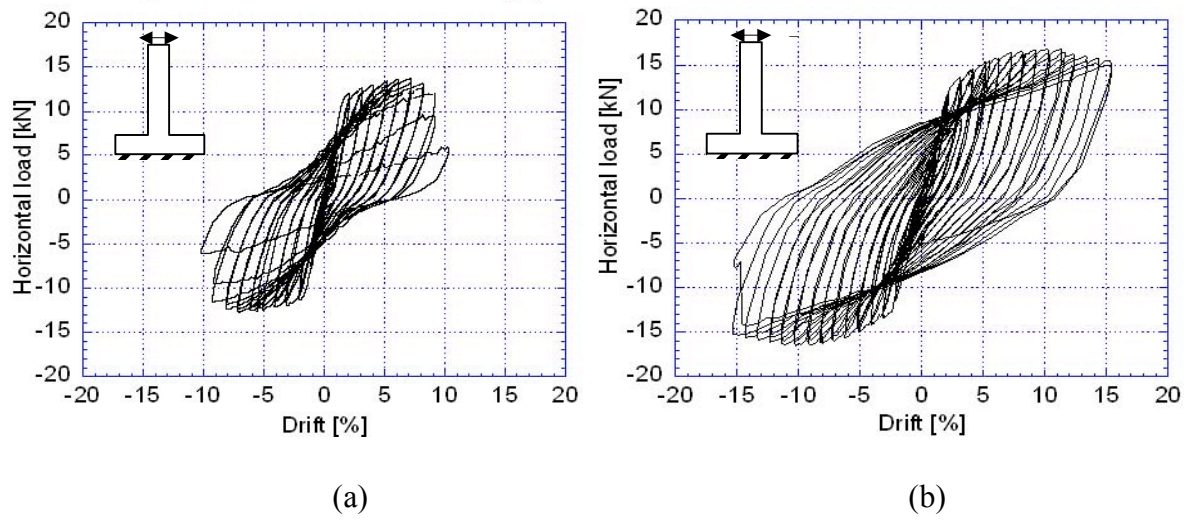


FIGURE 24.12: Hysteretic behavior of flexural members under fully reversed cyclic loading for (a) R/C with stirrups, and (b) R/ECC without stirrups (Fischer and Li, 2002a).

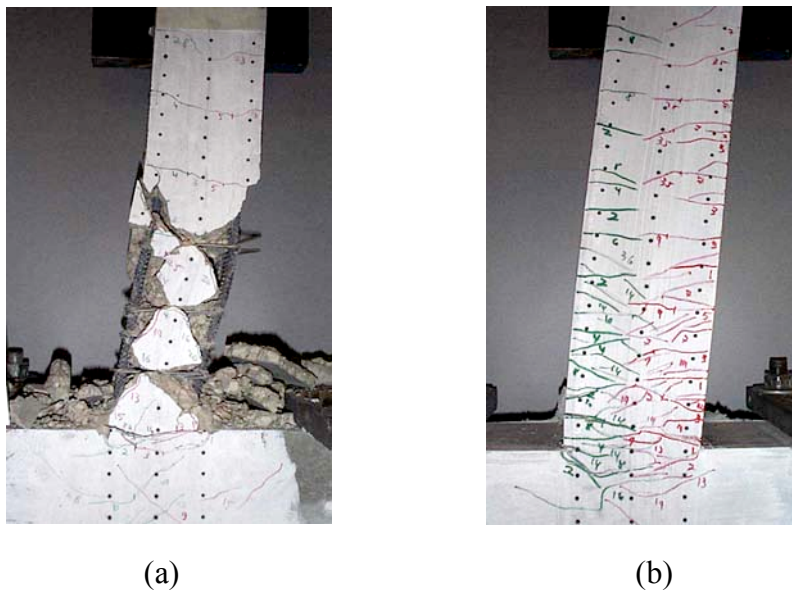


FIGURE 24.13: Damage behavior of (a) R/C and (b) R/ECC without stirrups, shown at 10% drift (Fischer and Li, 2002a).



FIGURE 24.14: Flexural fatigue testing of ECC link-slab element (Kim et al, 2004).

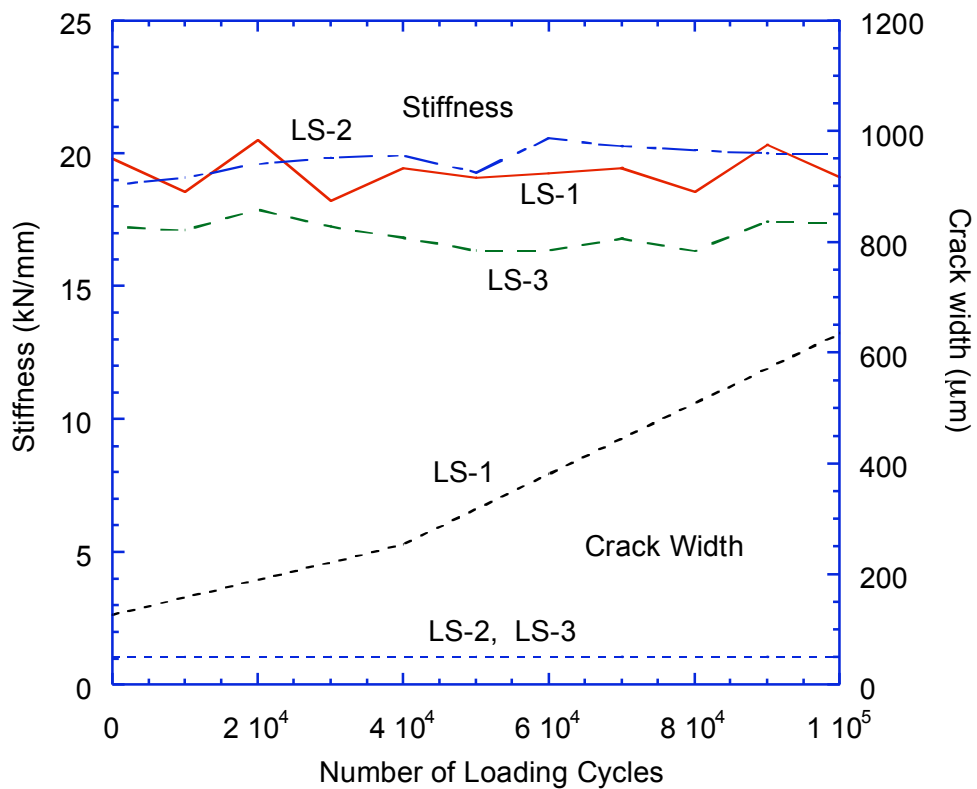


FIGURE 24.15: Stiffness and crack width change as a function of load cycles. LS-1 is the control R/C specimen. LS-2 and LS-3 are both R/ECC specimens with different reinforcement details to represent new and retrofit construction conditions (Kim et al, 2004).

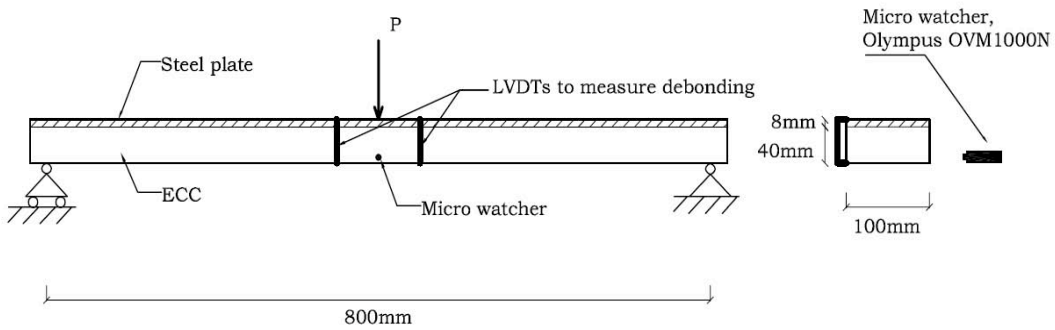


FIGURE 24.16: Composite steel/ECC beam test set-up (Walter et al, 2005).

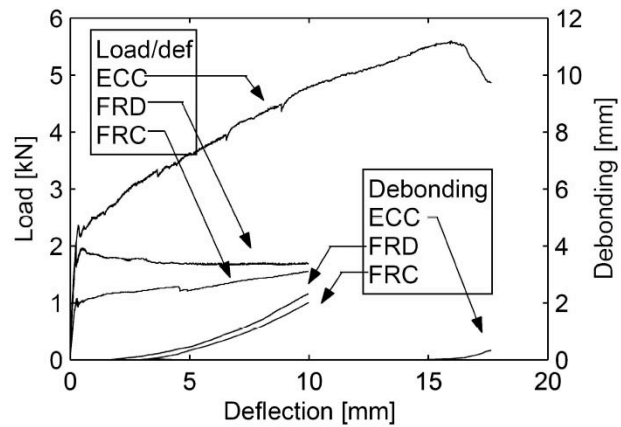


FIGURE 24.17: Load and debonding as a function of composite beam deflection (Walter et al, 2005). Significant increase in load capacity and delay in debonding was achieved in the steel/ECC beam versus the steel/FRC and steel/FRD beams.

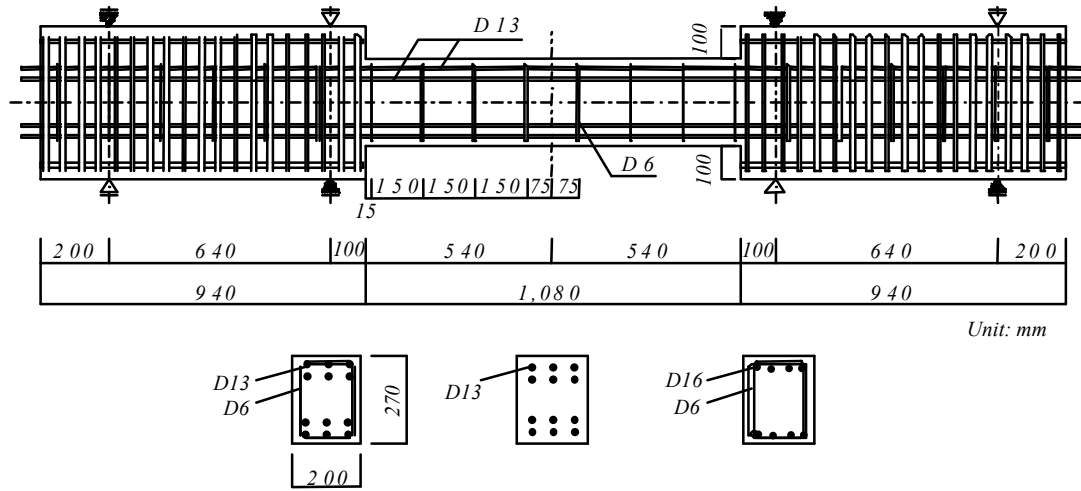
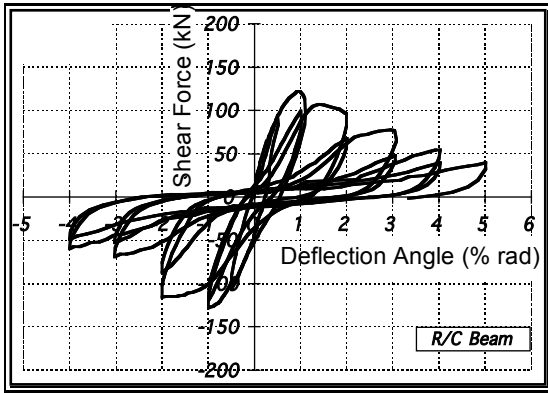
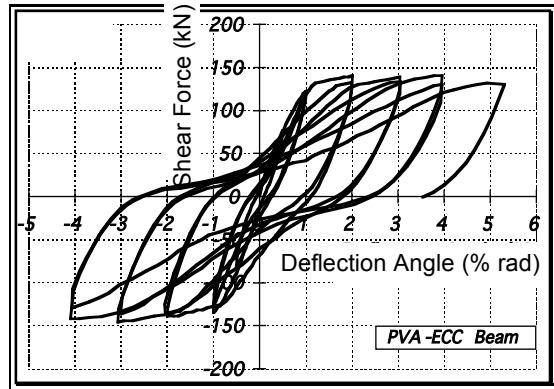


FIGURE 24.18: Fully reversed Ohno shear test set-up (Fukuyama et al, 2000).

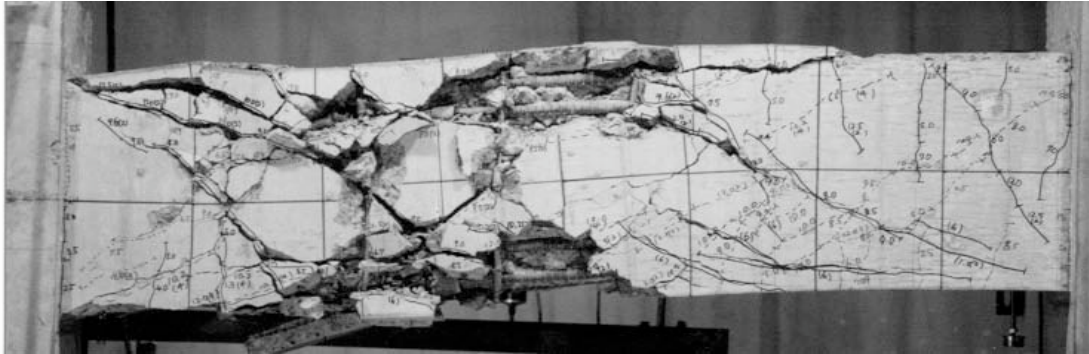


(a)

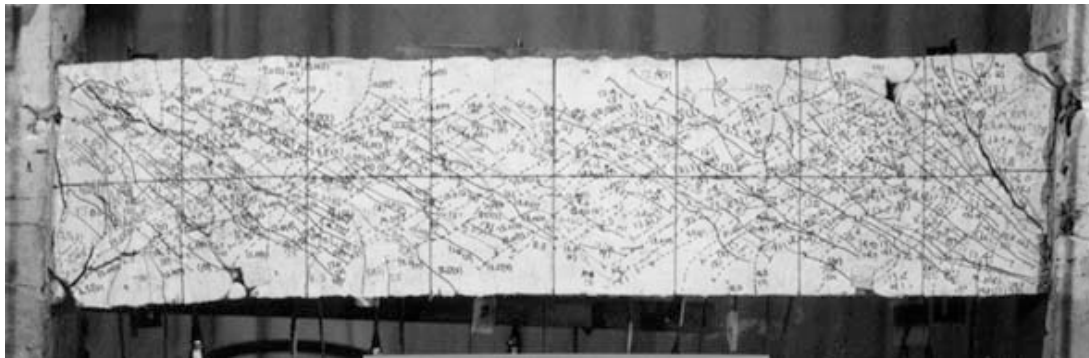


(b)

FIGURE 24.19: Hysteretic loops for Ohno shear beams under fully reversed cyclic loading for (a) R/C, and (b) R/ECC (Fukuyama et al, 2000).



(a)



(b)

FIGURE 24.20: Damage pattern in Ohno shear beams (a) R/C, and (b) R/ECC (Fukuyama et al, 2000).

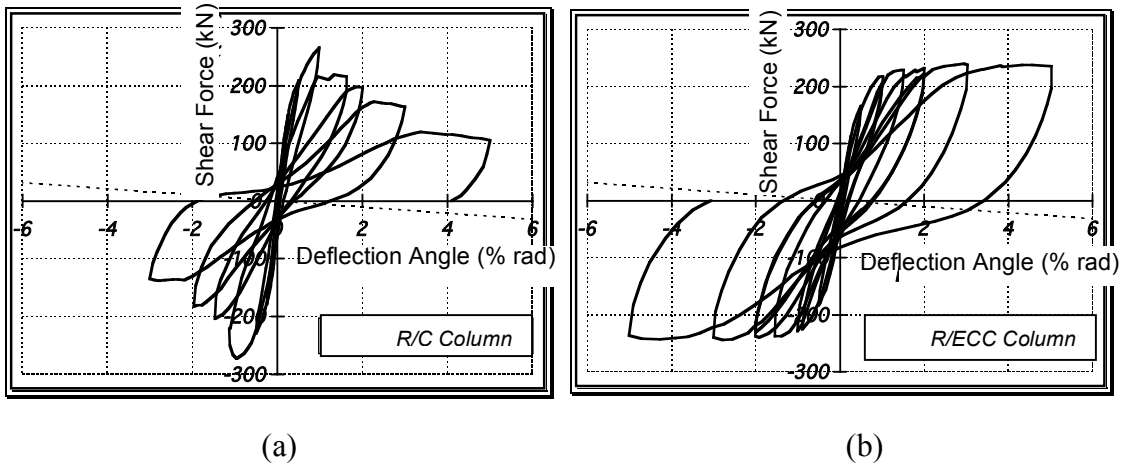


FIGURE 24.21: Hysteretic behavior of columns under fully reversed cyclic loading for (a) R/C, and (b) R/ECC (Fukuyama et al, 2000).

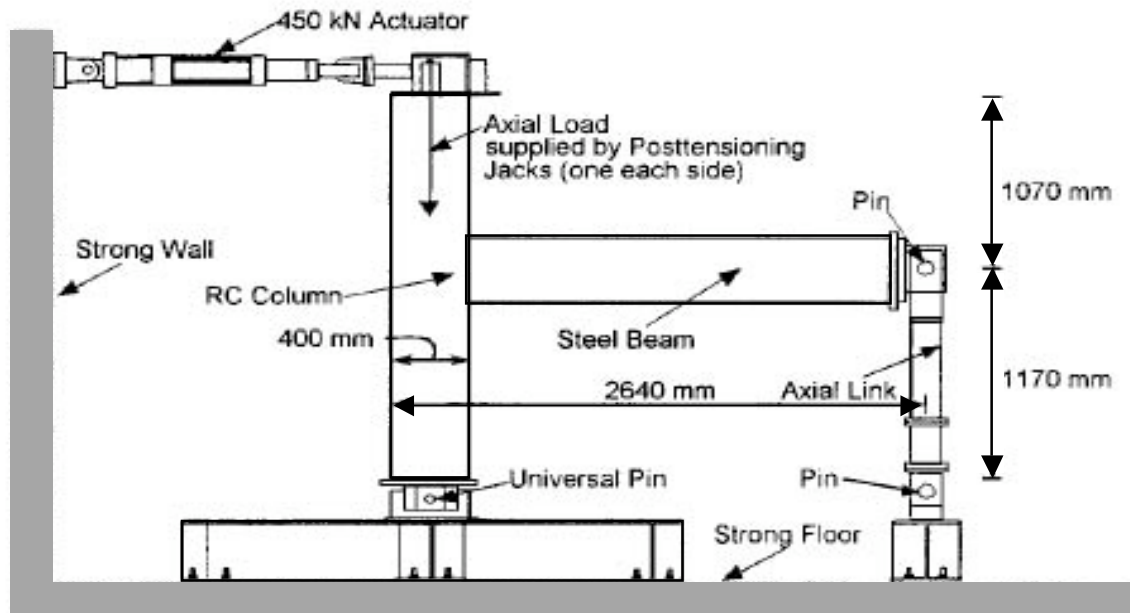
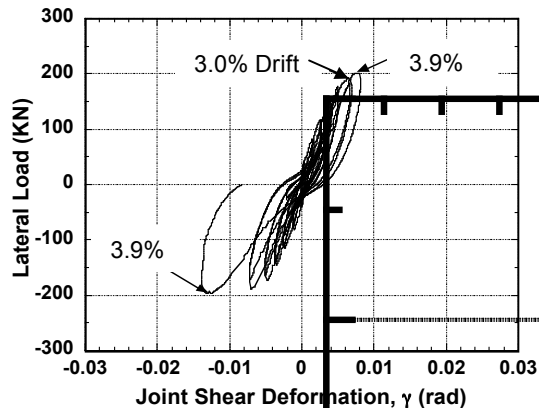
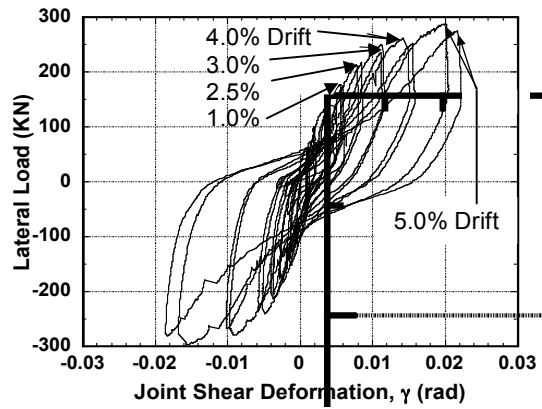


FIGURE 24.22: Test set-up for beam-column connection (Parra-Montesinos and Wight, 2000).



(a)



(b)

FIGURE 24.23: Hysteretic loops of fully reversed cyclic test on beam-column connections for (a) R/C with stirrups and (b) R/ECC without stirrups (Parra-Montesinos and Wight, 2000).

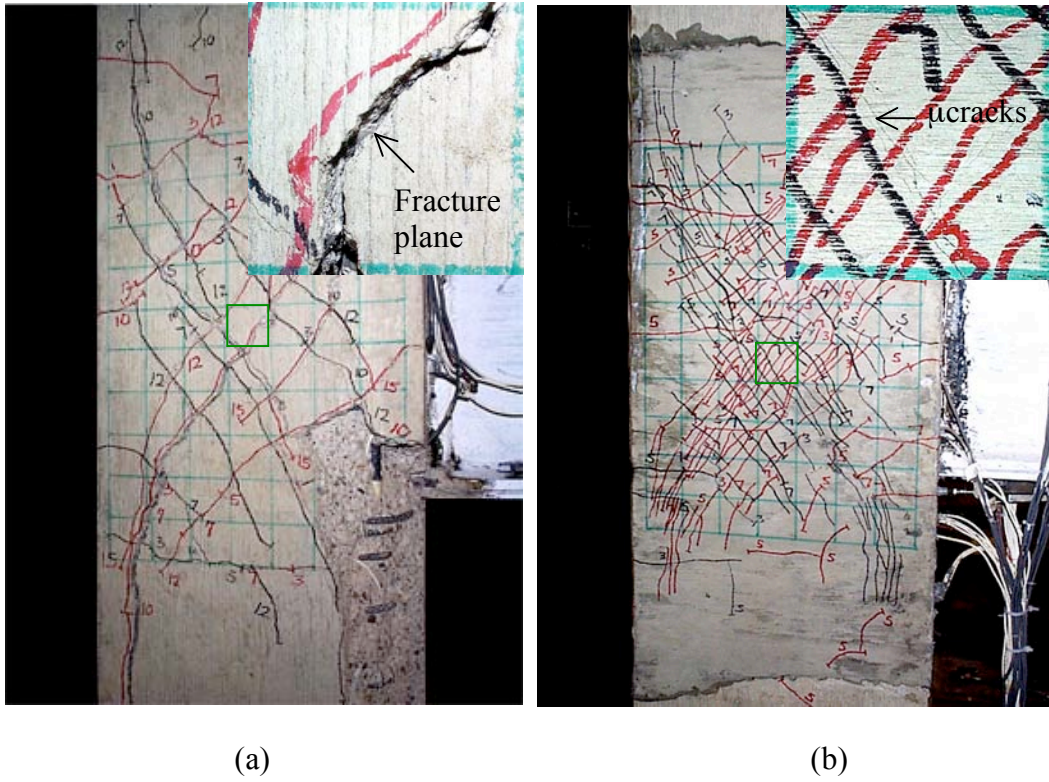


FIGURE 24.24: The damage behavior of the shear panel of a hybrid connection after cyclic loading (after Parra-Montesinos and Wight 2000). The green squares is enlarged in the inserts for easier viewing of the cracks in (a) R/C, and (b) R/ECC.

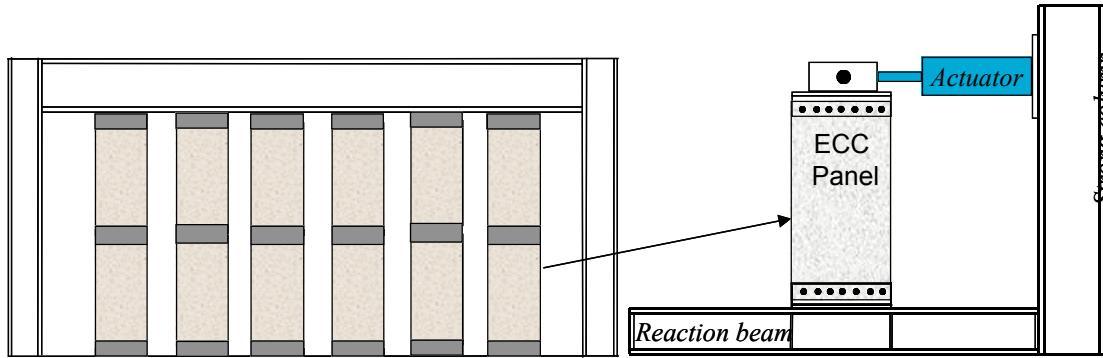


FIGURE 24.25: Wall panel test setup (Kesner and Billington, 2005).

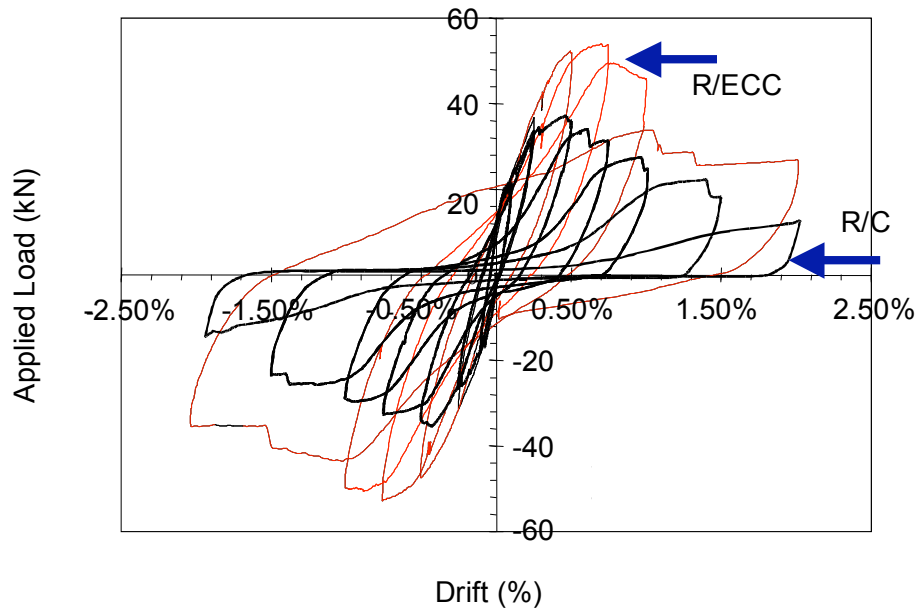
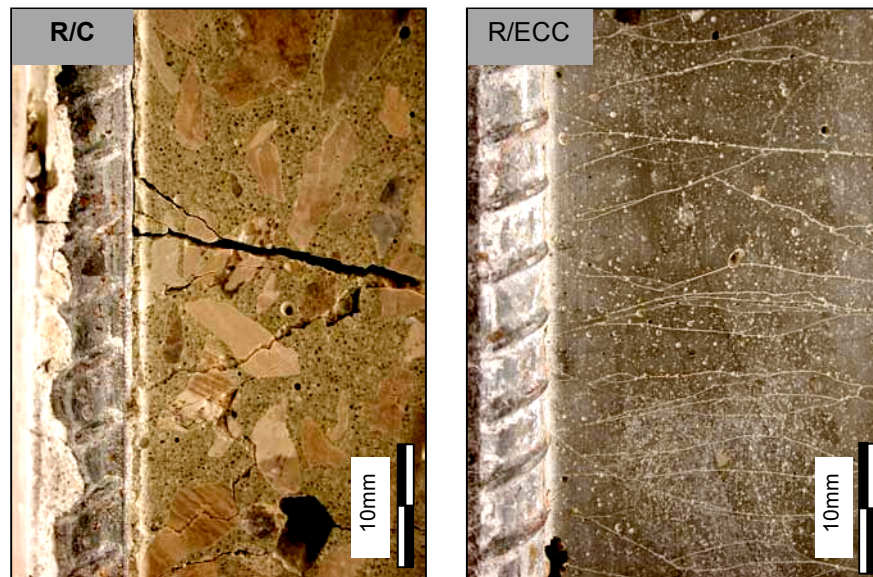
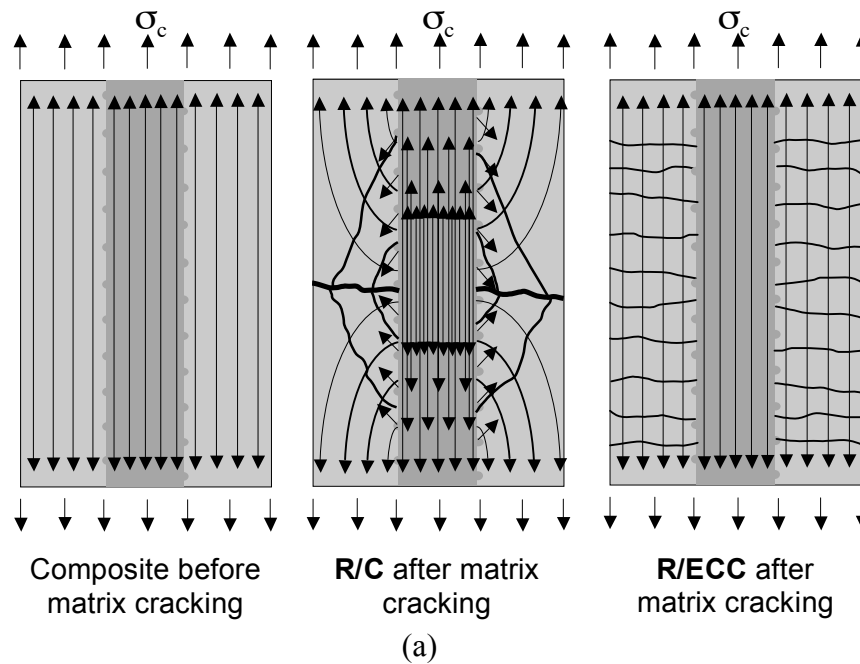


FIGURE 24.26: Hysteretic loops of shear wall (after Kesner and Billington, 2005).



(b)

FIGURE 24.27: (a) Stress flow before and after matrix cracking, and (b) Left: Brittle fracture of concrete in normal R/C causes unloading of concrete near crack, and a jump in tensile straining the steel locally, resulting in high interfacial shear and bond breakage. Right: In contrast, compatible deformation occurs between ECC and steel reinforcement with no shear lag, thus maintaining integrity of the interfacial bond. (Fischer and Li, 2002b).

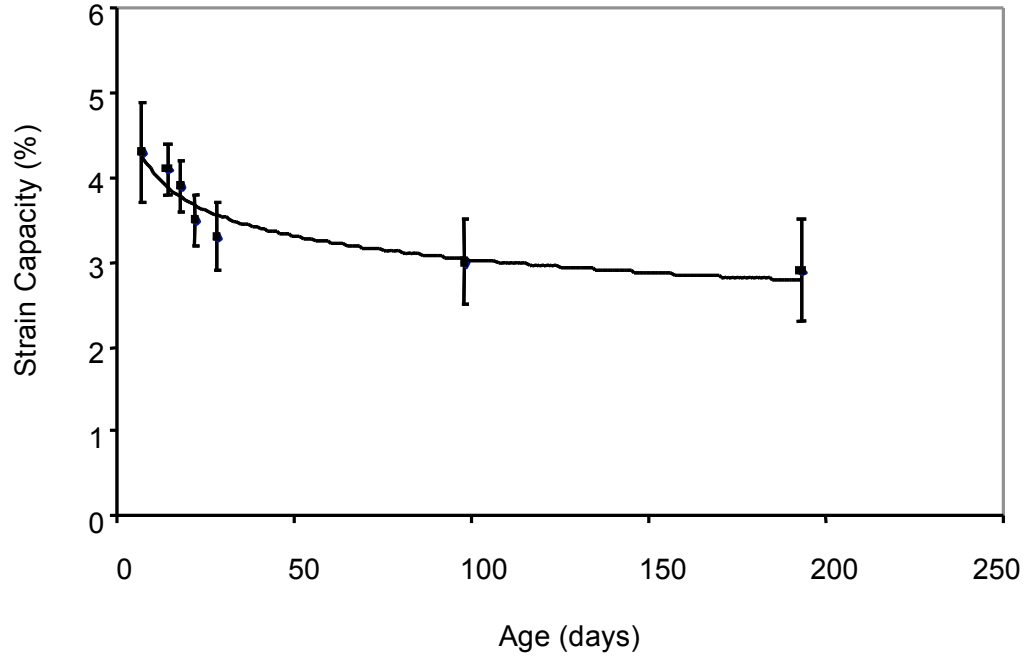


FIGURE 24.28: Tensile strain capacity of ECC as a function of age after casting (Li and Lepech, 2004).

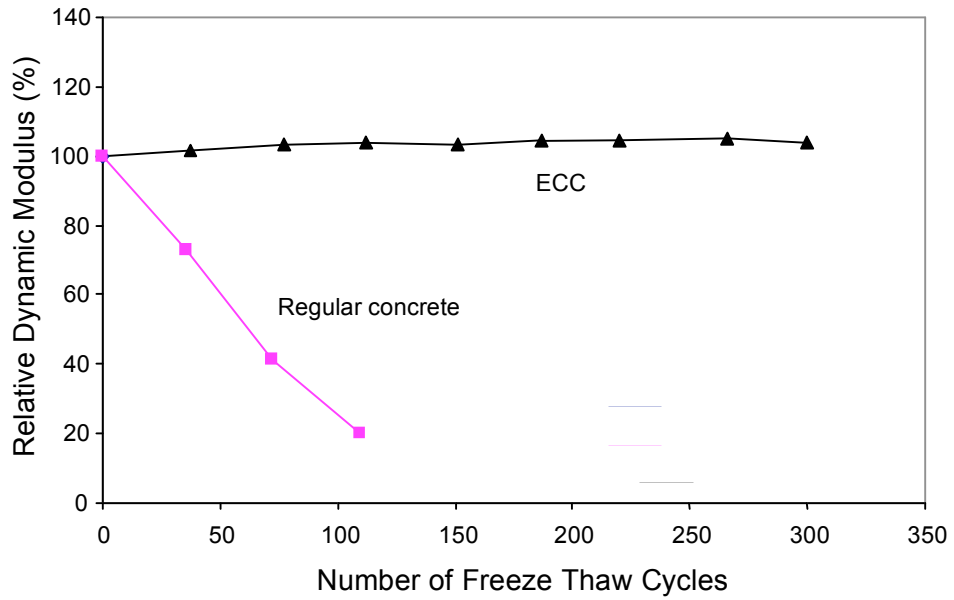


FIGURE 24.29: Relative dynamic modulus of normal concrete and three versions of ECC, all without air-entrainment (Li et al, 2003).

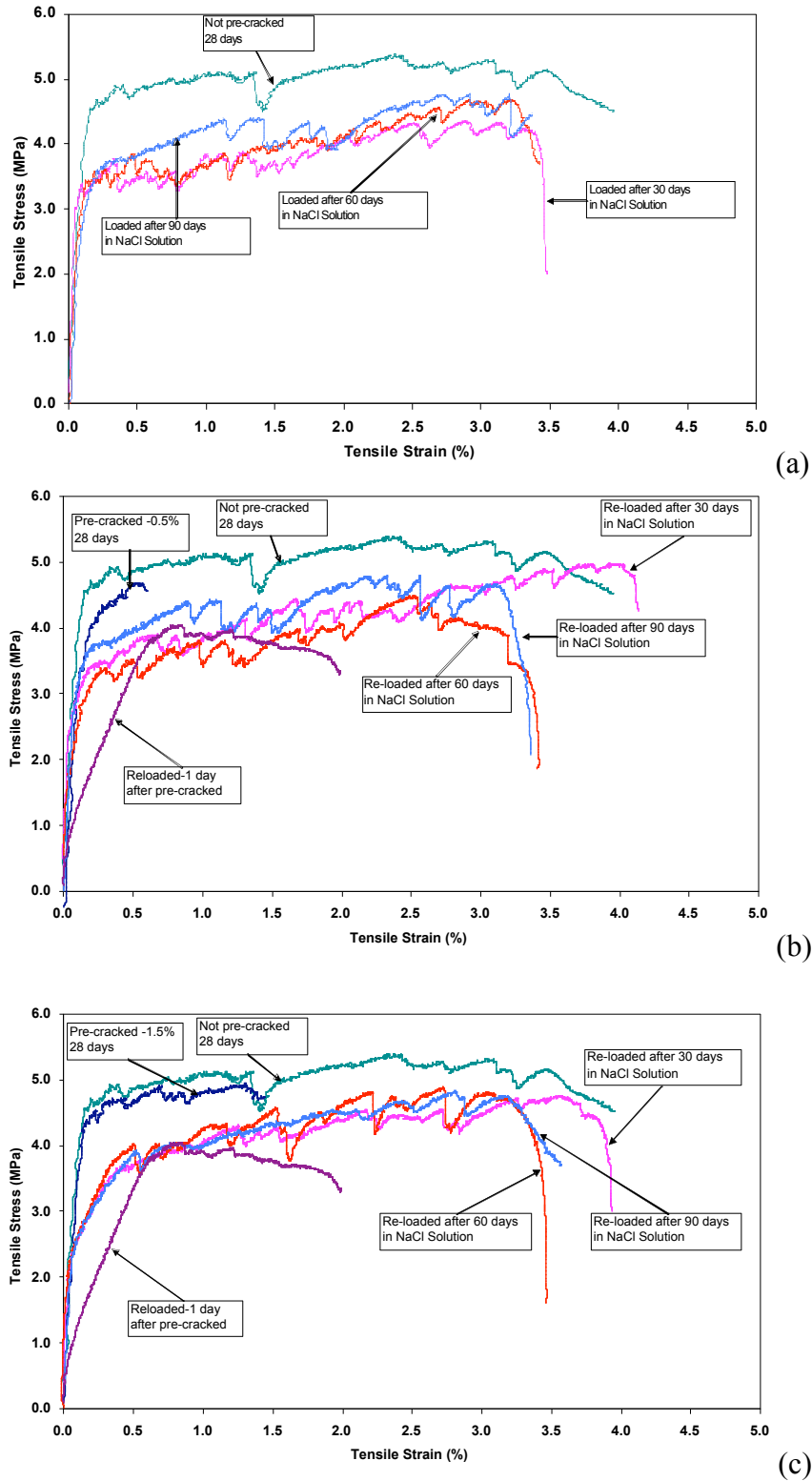
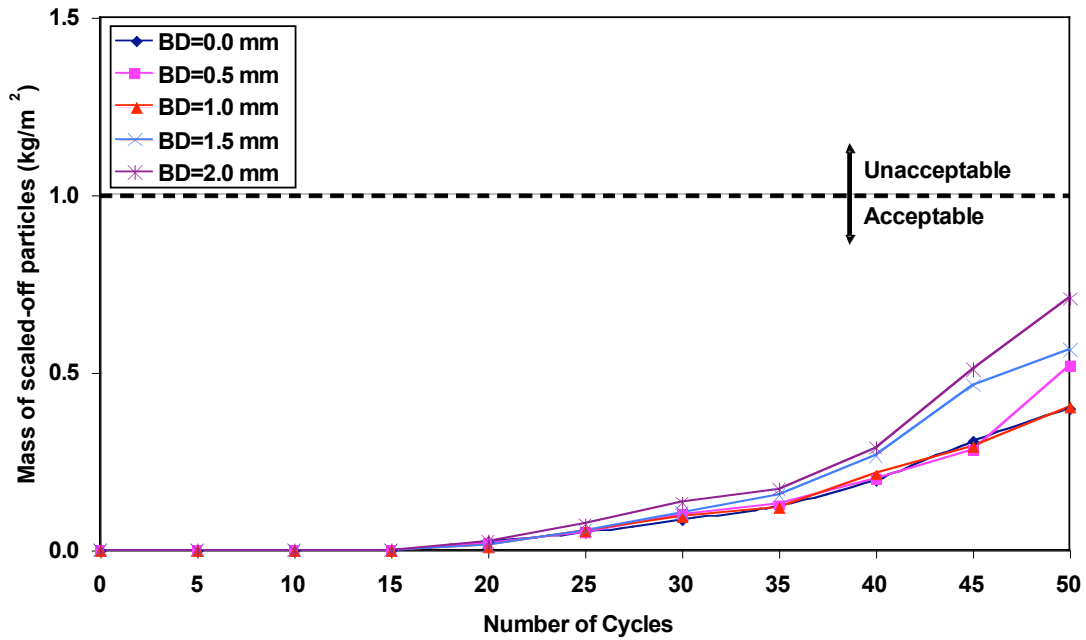
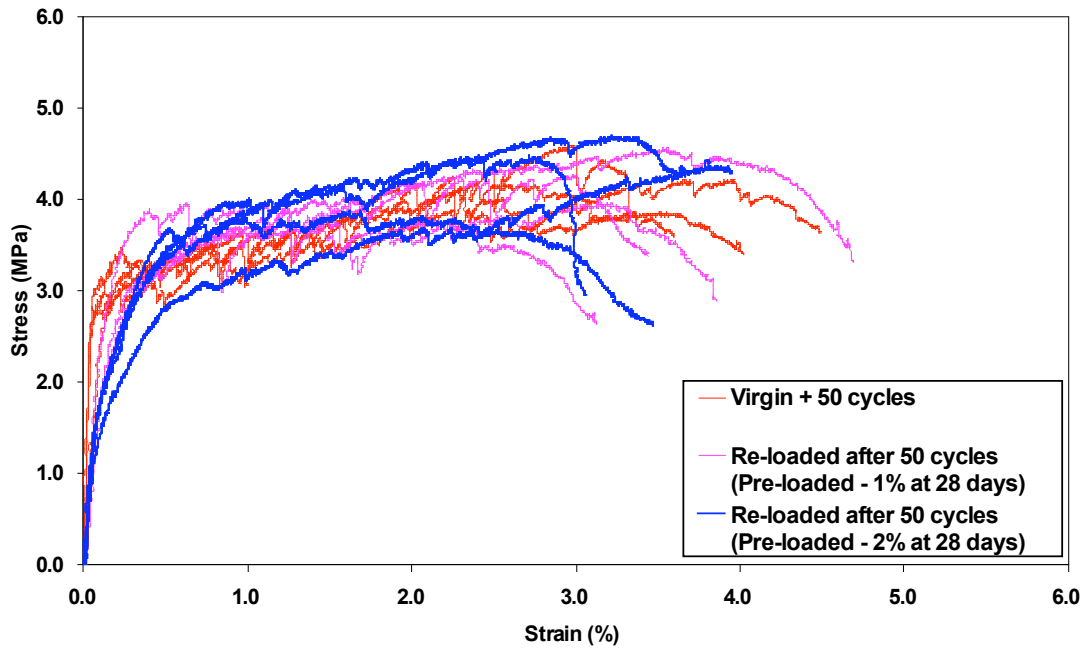


FIGURE 24.30: Tensile stress strain curves of ECC (a) virgin coupon specimens and (b) pre-cracked (to 0.5%) specimens and (c) precracked (to 1.5%) specimens, before and after subjected to 3% NaCl solution exposure (Li et al, 2007).

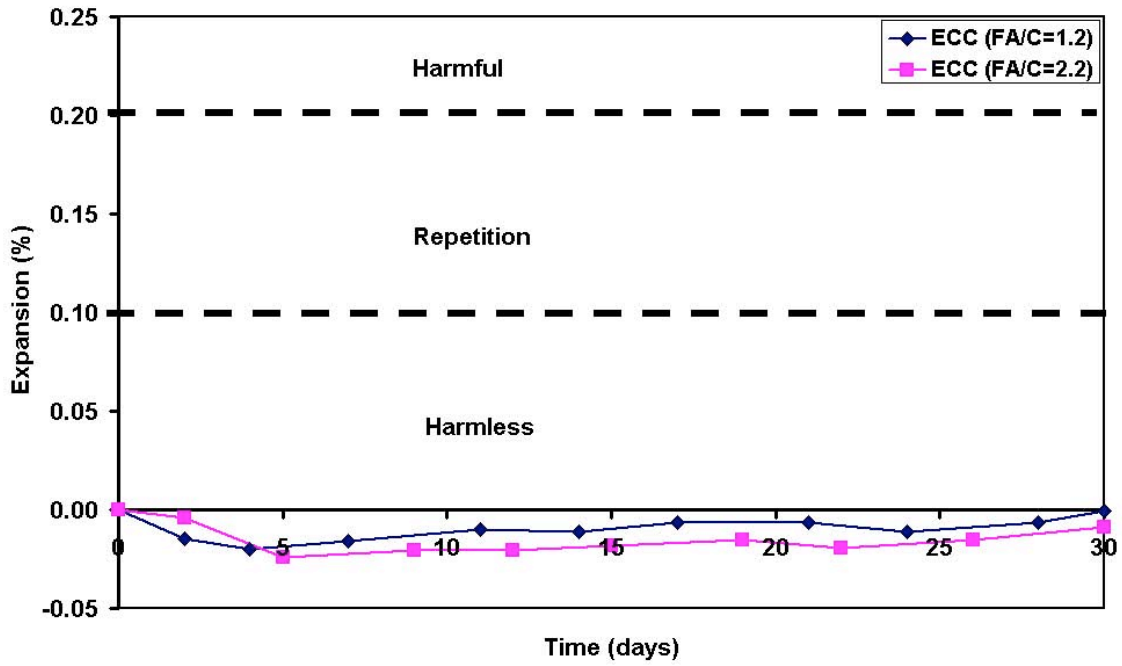


(a)

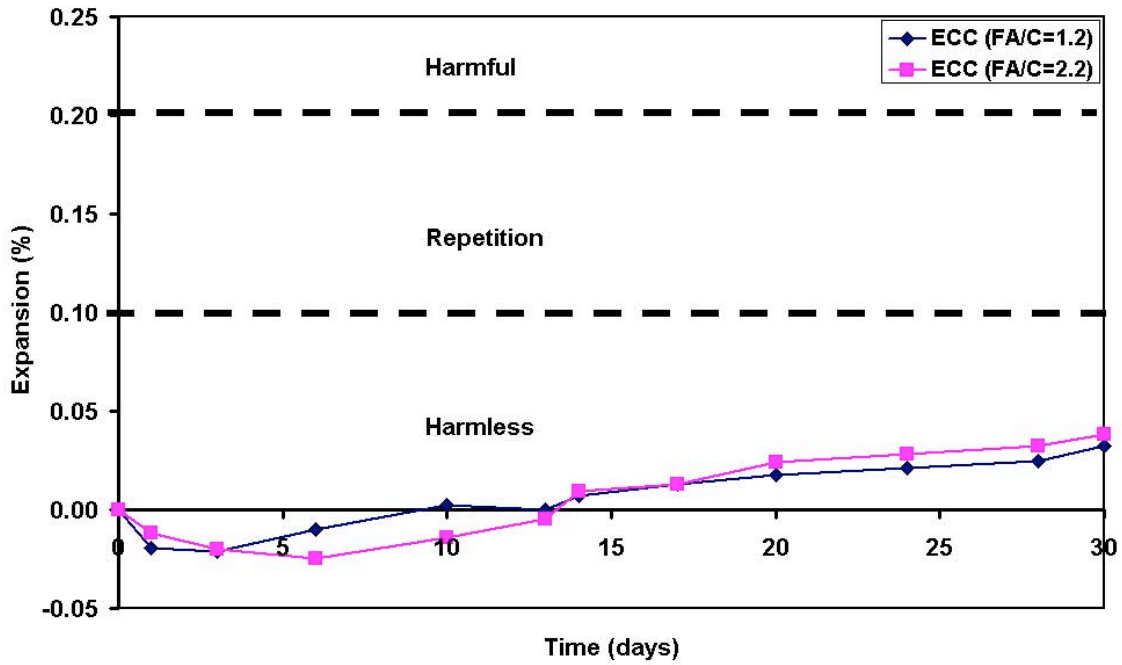


(b)

FIGURE 24.31: Effect of freeze-thaw cycles in the presence of de-icing salts for (a) beams preloaded to different bending deformation (BD) levels, showing mass of scaled-off particles, and (b) Coupon specimens preloaded to different levels, showing uniaxial tensile stress-strain curves after 50 cycles of exposure (Şahmaran and Li, 2007a).



(a)



(b)

FIGURE 24.32: Length Change of ECC Mix (a) with Class F fly ash, and (b) with Class C fly ash subjected to alkali-silicate reaction tests (Şahmaran and Li, 2007b).

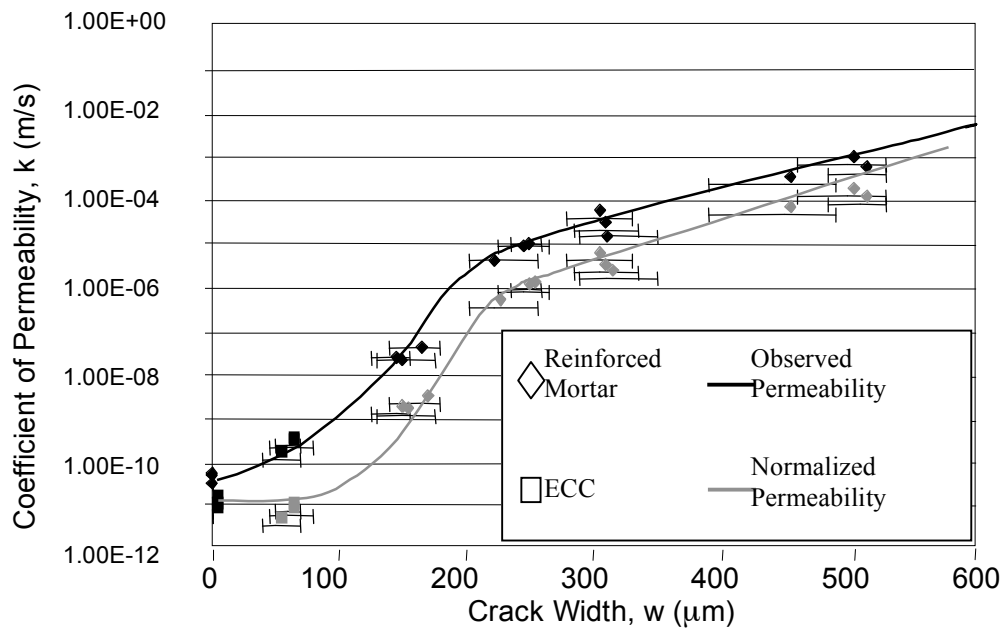


FIGURE 24.33: Permeability of precracked ECC and reinforced mortar measured as a function of crack width (after Lepech and Li, 2005).

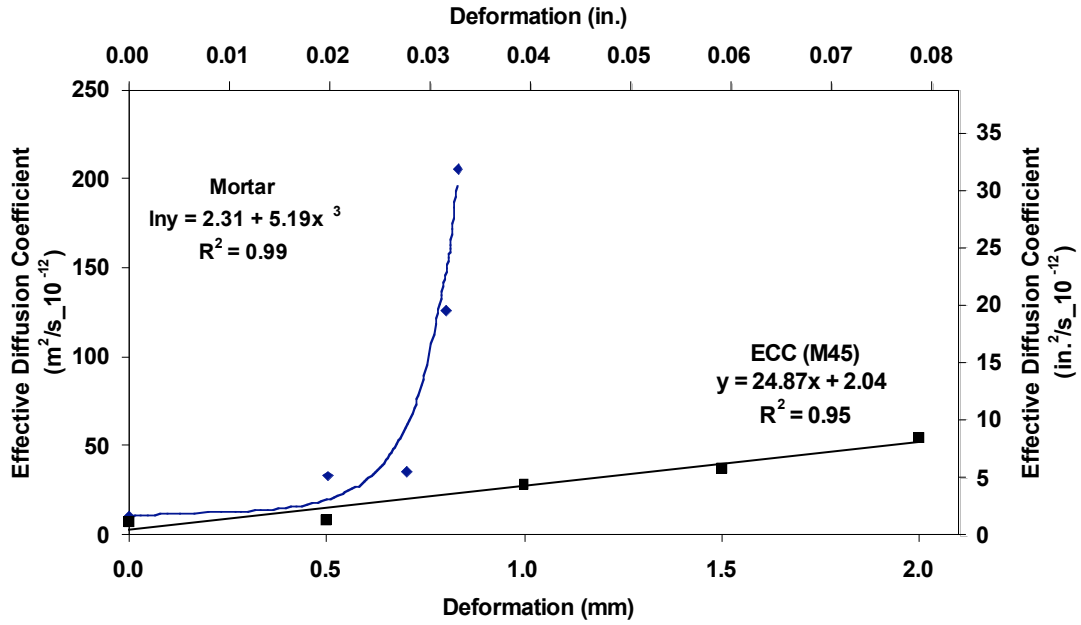
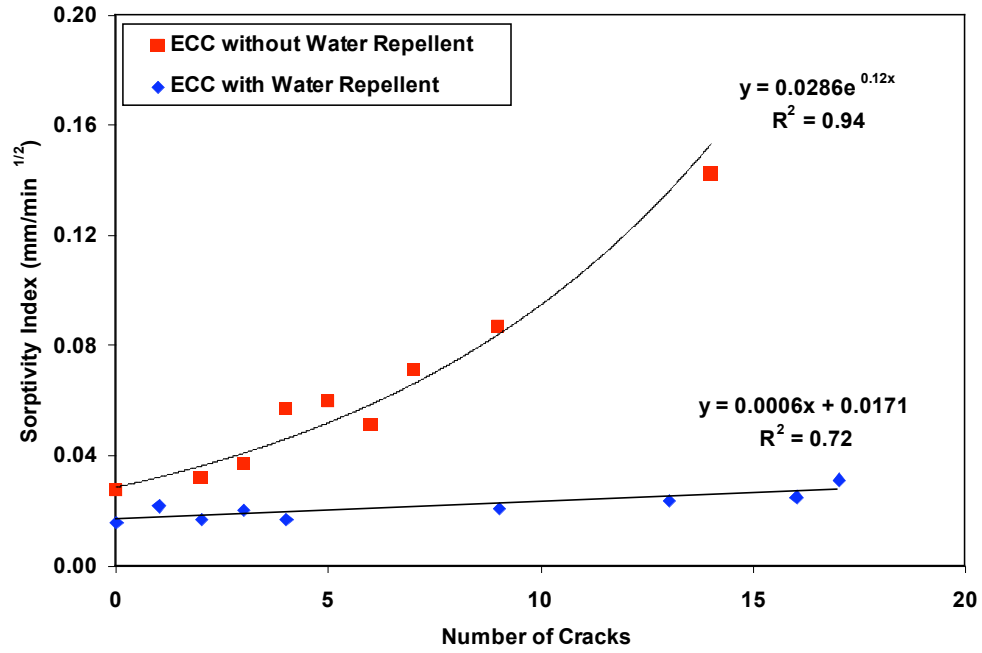
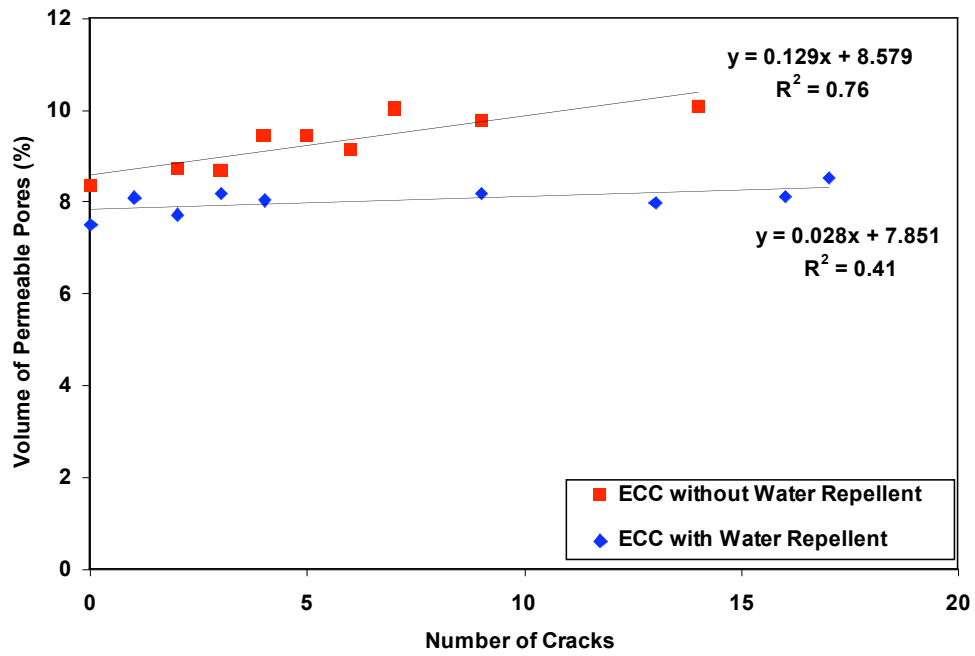


FIGURE 24.34: Diffusion coefficient versus pre-loading deformation level for ECC and mortar (Şahmaran et al, 2007).



(a)



(b)

FIGURE 24.35: Capillary transport properties measured for preloaded ECC beams, showing the effects of water repellent on (a) Sorptivity index and (b) Volume of permeable pores, as a function of the number of cracks (Şahmaran and Li, 2007c).

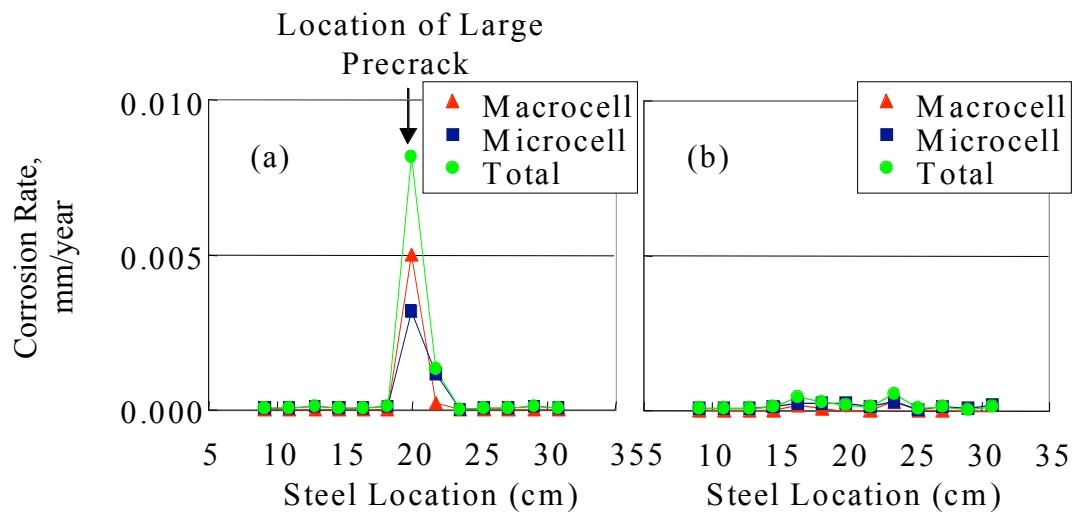
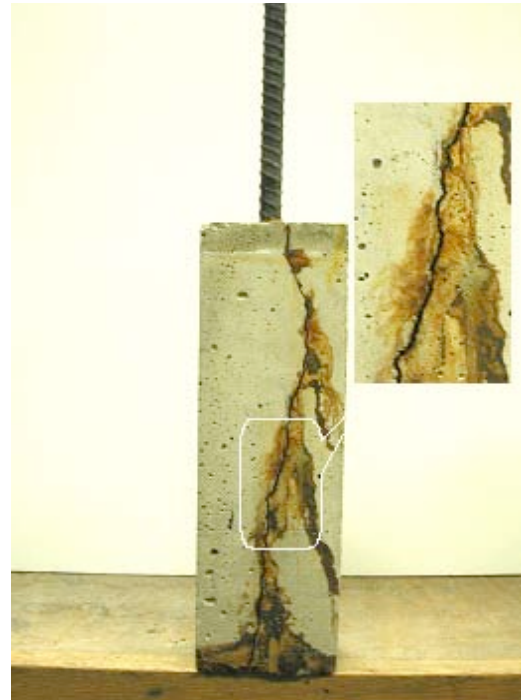


FIGURE 24.36: Measured corrosion rate along the steel rebar for preloaded (a) R/C, and (b) R/ECC (after Miyazato and Hiraishi, 2005).



(a)



(b)



(c)



(d)

FIGURE 24.37: ECC and mortar specimens after accelerated corrosion test: (a) ECC prismatic specimen after 300 hours accelerated corrosion, (b) Mortar prismatic specimen after 75 hours accelerated corrosion, (c) ECC cylindrical specimen after 350 hours accelerated corrosion, (d) Mortar cylindrical specimen after 95 hours accelerated corrosion (Şahmaran et al, 2006).

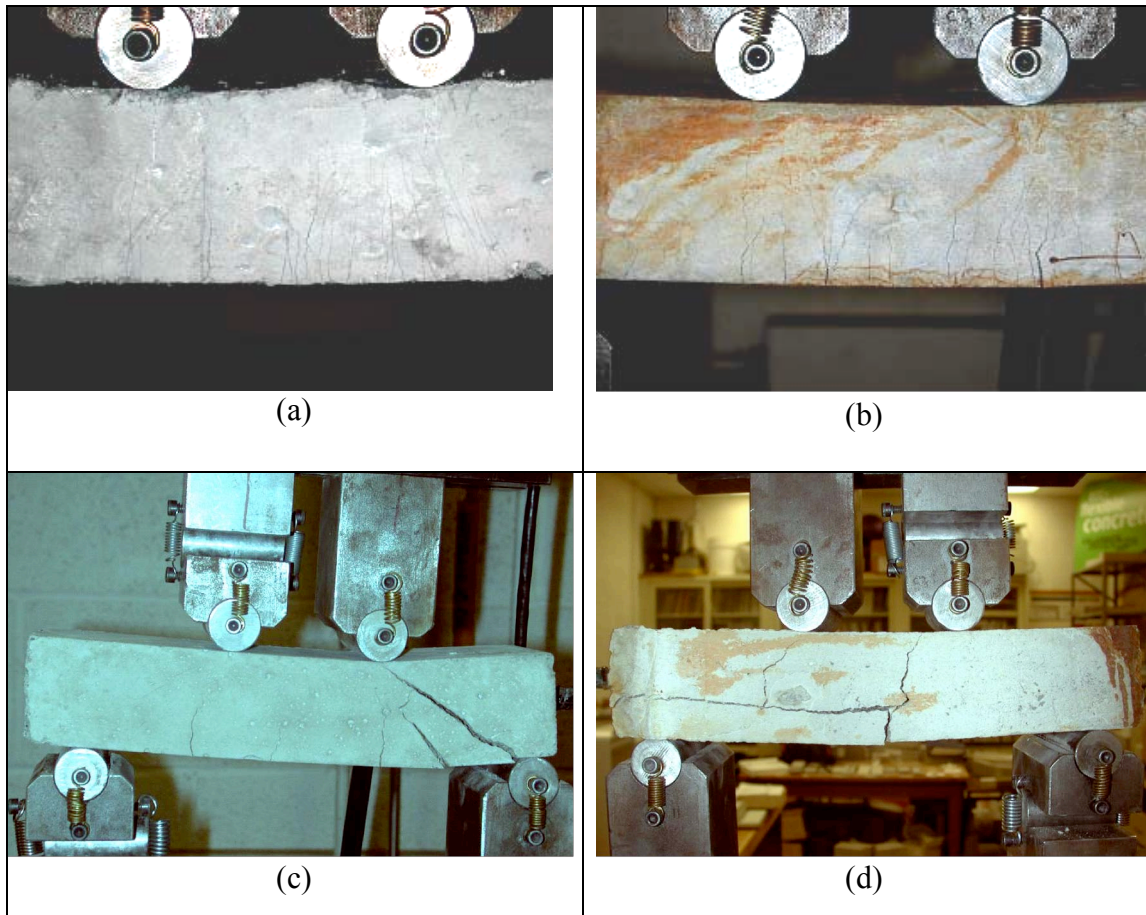


FIGURE 24.38: Types of failure of reinforced mortar and ECC beams under four point bending test for (a) ECC before accelerated corrosion, (b) ECC after 150 hours accelerated corrosion, (c) Mortar before accelerated corrosion, and (d) Mortar after 50 hours accelerated corrosion (after Şahmaran et al, 2006).

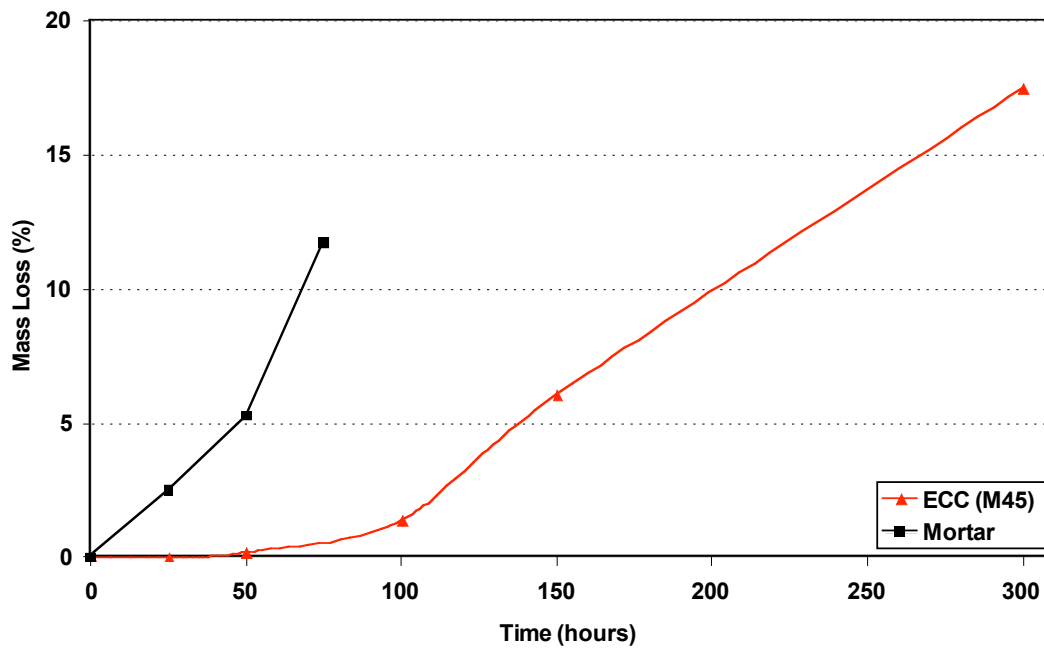
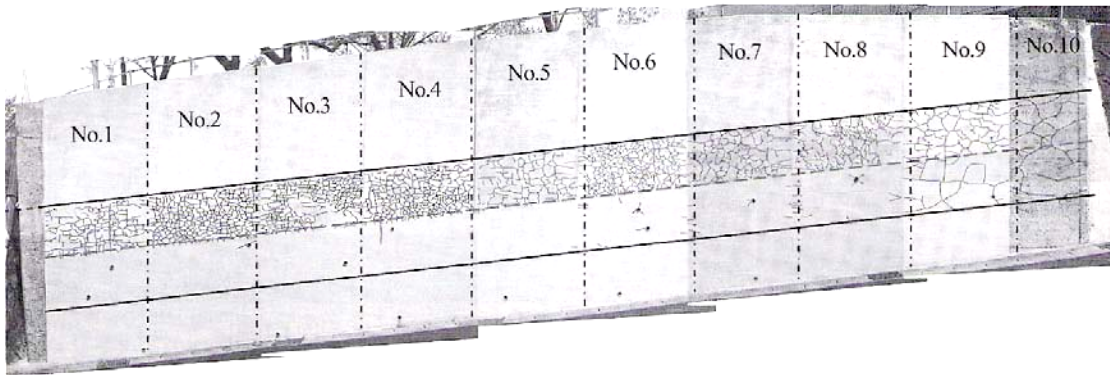


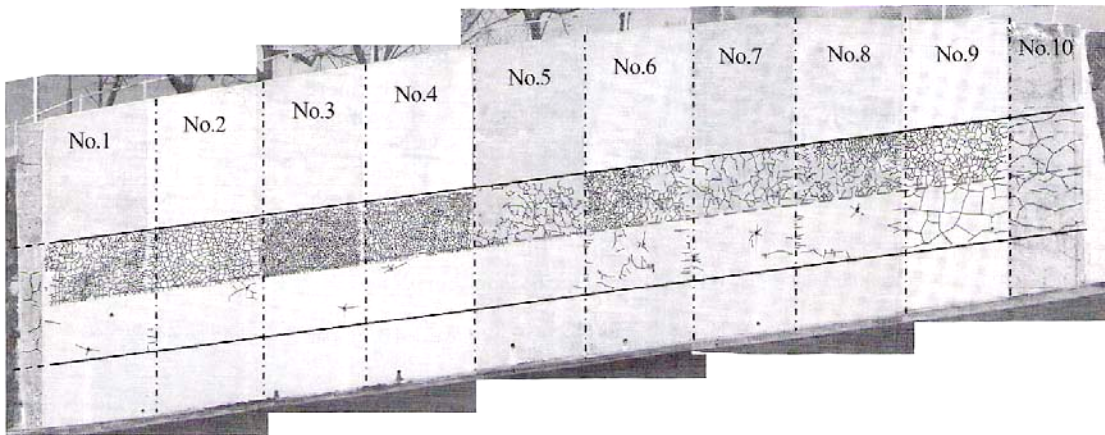
FIGURE 24.39: Mass loss versus time for ECC and mortar corrosion specimens (Şahmaran et al, 2006).



(a)



(b)

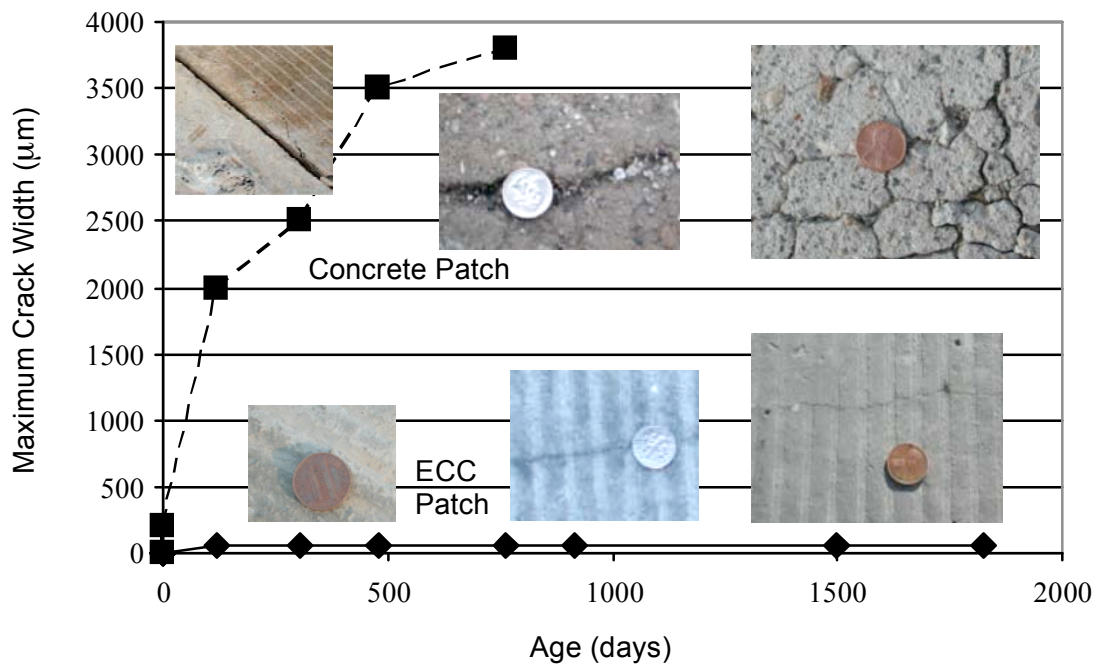


(c)

FIGURE 24.40: Cracking behavior of patched earth retaining wall (a) Before repair and showing ASR damage, and (b) after repair at 12 months, and (c) after repair at 24 months. Blocks 1-8 used ECC, block 9 use a normal repair mortar, and block 10 was left unrepaired (after Rokugo et al, 2005).



(a)



(b)

FIGURE 24.41: (a) ECC and concrete patches on the Curtis Road, Ann Arbor bridge deck, (b) Maximum crack width development over time for the two materials. The concrete patch was re-repaired at about 1000 days.